

Distribution of alkylamines in surface waters around the Antarctic Peninsula and Weddell Sea

Arianna Rocchi^{1,2}, Mark F. Fitzsimons³, Preston Akenga³, Ana Sotomayor⁴, Elisabet L. Sà¹, Queralt Güell-Bujons¹, Magda Vila¹, Yaiza M. Castillo¹, Manuel Dall'Osto¹, Dolors Vaqué¹, Charel Wohl^{1,5,6}, Rafel Simó¹ and Elisa Berdalet¹

¹Department of Marine Biology and Oceanography, Institute of Marine Sciences (ICM), CSIC, Barcelona, E-08003, Spain.

²Faculty of Earth Sciences, University of Barcelona, Barcelona, E-08028, Spain.

³Biogeochemistry Research Centre, School of Geography, Earth and Environmental Sciences, University of Plymouth, Plymouth, PL4 8AA, UK.

⁴Marine Technology Unit (UTM), CSIC, Pg Marítim de la Barceloneta, 37-49, Barcelona, E-08003, Spain.

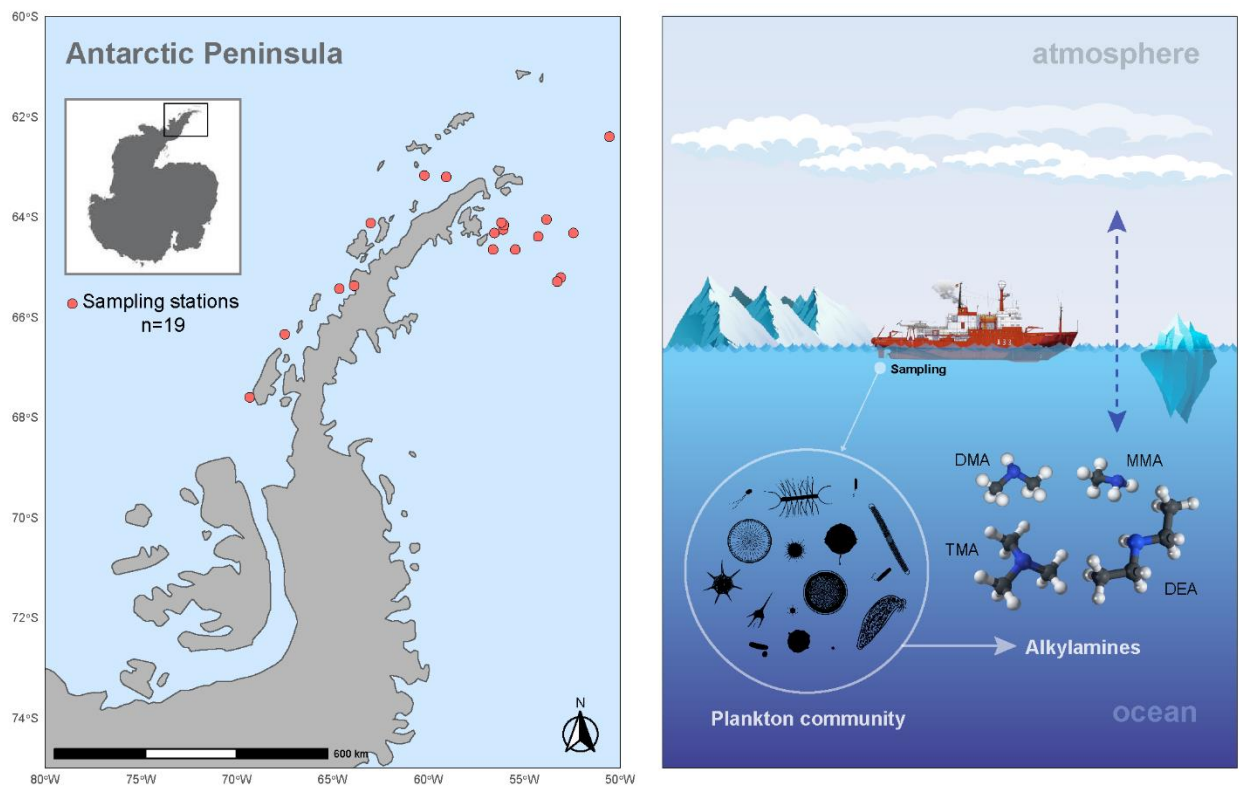
⁵Centre of Ocean and Atmospheric Sciences, School of Environmental Sciences, University of East Anglia, Norwich, NR4 7TJ, UK.

⁶National Centre for Atmospheric Science, University of East Anglia, Norwich, NR4 7TJ, UK.

Correspondence to: Arianna Rocchi (rocchi@icm.csic.es), Elisa Berdalet (berdalet@icm.csic.es)

Abstract. Alkylamines, volatile organic nitrogen compounds with small molecular weight, are present in the surface ocean, participate in the marine biogeochemical nitrogen cycle, atmospheric chemistry and cloud formation. Alkylamines have been detected in polar regions, suggesting that these areas constitute emission hotspots of these compounds. However, knowledge of the sea surface distribution patterns and factors modulating alkylamines remain limited due to their high reactivity and low concentrations, which hamper accurate measurements. We investigated the presence and distribution of alkylamines in seawaters around the Antarctic Peninsula and the northern Weddell Sea during the late austral summer and explored their potential links to marine microbiota. Alkylamines were ubiquitous in all analyzed samples, accounting for ~2 % of the dissolved and particulate organic nitrogen pool. The only particulate form found was trimethylamine (TMA), detected for the first time in Antarctic waters at concentrations of 9.7 ± 4.6 nM. We efficiently measured dissolved trimethylamine (TMA, 20.9 ± 15.2 nM), dimethylamine (DMA, 32.3 ± 32.7 nM) and diethylamine (DEA, 7.2 ± 1.7 nM) across the surveyed area, while dissolved monomethylamine (MMA, 12.7 ± 0.1 nM) remained below detection limit in most samples. Variations in alkylamine concentrations did not align with the overall phytoplankton biomass but with specific biological components. TMA was predominantly associated with, and released from, nanophytoplankton. DMA was likely produced by the degradation of TMA or trimethylamine oxide by nanophytoplankton cells or associated

heterotrophic bacteria. The sources of DEA remain unclear but were suggestive of a distinct biogeochemical pathway from those of TMA and DMA. MMA is thought to primarily originate from bacterial degradation of nitrogen-based osmolytes or amino acids, but detection in too few samples precluded any robust association with microbiota. This study reveals that volatile alkylamines are widespread in Antarctic surface waters, where they are primarily sourced from nanophytoplankton cells and associated heterotrophic bacteria and protists.



Short summary. During the PolarChange expedition, volatile alkylamines, important players in nitrogen cycling and cloud formation, were measured in Antarctic waters using a high-sensitivity method. Trimethylamine was the dominant alkylamine in marine particles, associated with nanophytoplankton. Dissolved dimethylamine likely originated from trimethylamine degradation, while diethylamine sources remain unclear. These findings confirm the biological origin of alkylamines in polar marine microbial food webs.

1 Introduction

The marine organic nitrogen (ON) pool is an important natural reservoir of reactive molecules, containing biologically relevant compounds which contribute to biogeochemical cycles in the surface ocean and ocean-atmosphere-climate interactions. Among them, alkylamines are low-molecular weight (<100 Da) polar molecules that exhibit high solubility in seawater and high vapor pressure. Alkylamines are emitted from the ocean to the atmosphere 1) via sea spray, contributing to a highly variable nitrogen-containing fraction of primary aerosols (Dall'Osto et al., 2017; Liu et al., 2022), and 2) through gas exchange, where they are efficiently incorporated into secondary marine aerosols and contribute to very fast new particle formation events (Brean et al., 2021; Corral et al., 2022; Ning et al., 2022; Zu et al., 2024). Additionally, Antarctic sea-ice microbiota and sea-ice-influenced ocean systems are significant sources of dissolved organic nitrogen (DON), including alkylamines, to both the ocean and the atmosphere, with notable release during sea-ice melt (Dall'Osto et al., 2017, 2019; Rinaldi et al., 2020).

Despite recent efforts, the quantification of these species in seawater remains a considerable challenge due to their low concentrations and reactivity (Fitzsimons et al., 2023), which hampers understanding of their concentrations in both dissolved and particulate forms. In the ocean, the main alkylamines reported are the class of methylamines (MAs), which exist in primary (monomethylamine, MMA: CH_3NH_2), secondary (dimethylamine, DMA: $(\text{CH}_3)_2\text{NH}$), and tertiary (trimethylamine, TMA: $(\text{CH}_3)_3\text{N}$) forms, plus diethylamine (DEA: $(\text{CH}_3\text{CH}_2)_2\text{NH}$), a secondary amine with two ethyl groups bound to the amino nitrogen (N) (Goldwhite, 1964). Amine concentrations in seawater are determined by biogeochemical processes, including production and consumption by marine microorganisms (Gibb et al., 1999). Phytoplankton, other protists and bacteria release N-containing compounds such as proteins, amino acids and several forms of amines (Poste et al., 2014) via organism excretion, cell death or lysis. Some of these compounds are directly synthesized by phytoplankton and used as osmolytes for regulating cellular homeostasis in response to salinity variations (Burg and Ferraris, 2008), and as cryoprotectants (Fitzsimons et al., 2024). The precursors for alkylamines are glycine betaine, choline, trimethylamine N-oxide (TMAO), and quaternary amines (R_4N^+). These N- (and Carbon, C) containing molecules are progressively degraded to TMA by bacteria, followed by further degradation into the less methylated compounds, DMA and MMA (Lidbury et al., 2015a, b; Mausz

and Chen, 2019; Sun et al., 2019). This displays similarities to the ocean sulfur cycle of dimethylsulfoniopropionate and dimethylsulfide (DMSP and DMS, respectively) (Stefels, 2000). Marine bacteria and archaea can use alkylamines as a source of energy and remineralize the organic N to ammonium (Landa et al., 2017; Lidbury et al., 2015a; Mausz and Chen, 2019).

The few available studies showed that alkylamines represent a small and highly variable percentage of marine ON compounds in the ocean (Fitzsimons et al., 2023, 2024 and references therein). The presence of alkylamines in seawater can have ecological implications, serving as nutrients (C and N sources) for marine microbiota, thereby influencing primary production and ecosystem dynamics (Chistoserdova et al., 2009; Palenik and Morel, 1991; Taubert et al., 2017). For instance, in tropical waters van Pinxteren et al. (2019) found an association between alkylamines and biological tracers such as chlorophyll-a and fucoxanthin, suggesting that they were produced by marine diatoms. Furthermore, Koester et al. (2022) hypothesised that the broad array of N metabolites plays a significant role in the interactions between the diatom *Pseudo-nitzschia* and its bacterial microbiome (particularly *Polaribacter*), thus contributing fundamentally to the ecophysiology of the diatom. Also, Suleiman et al. (2016) showed that interactions between diatoms and heterotrophic bacteria may be important for marine amine cycling. Investigations into the co-occurrence and abundance of proteobacteria, diatoms and MAs in the marine water column have uncovered interkingdom cross-feeding, underscoring the previously underestimated significance of MAs in the marine N and C cycles (Stein, 2017). Moreover, MAs share a bacterial oxidation pathway with the climate-relevant sulfur gas DMS into dimethylsulfoxide (DMSO) (Lidbury et al., 2016). DEA has been previously found in seawater (Poste et al., 2014; Van Pinxteren et al., 2012, 2019; Fitzsimons et al., 2024) and marine aerosols (Facchini et al., 2008; Dall'Osto et al., 2019). However, no information exists on production pathways, potential biological precursors, or transformation processes in seawater. In summary, the amine cycle in the ocean is related to several microbial processes, which this study sought to explore further.

Here we aimed to investigate the presence, distribution, and potential sources of alkylamines in Antarctic waters and to enhance our understanding of how these compounds are linked to polar microbial ecology. To achieve this, we visited the Southern Ocean near the Antarctic coasts, one of the most pristine environments on Earth, which is a source of ON (Dall'Osto et al., 2017) and serves as a proxy for preindustrial marine conditions. Surface waters around the Antarctic

Peninsula were analysed using a sensitive and robust method specifically designed for detecting low molecular weight aliphatic amines. We characterized in detail the biogeochemical properties and microbial composition of the same waters to explore the drivers of alkylamine distribution.

2 Methods and Material

2.1 Study area and sampling strategy

The PolarChange (Aerosol Emissions in Changing Polar Environments) expedition was conducted on board the RV *Hesperides* in the Southern Ocean around the Antarctic Peninsula, during late austral summer from the 14th of February to the 17th of March 2023. During this cruise, we collected surface seawater samples from the underway water inlet (~4 m deep) to analyse for amines (dissolved and particulate forms) and accompanying microbiota and biogeochemical parameters. Seven stations were located in the western side of the Antarctic Peninsula, and twelve in the eastern side, within the Weddell Sea area (Fig. 1, Table S1). Seawater was obtained at 18:00 (local time), except for samples #2 and #18, which were collected at 12:00 mid-day. Sea surface water temperature (°C) (SST), salinity and density (sigmaT) were measured by the probe SeaBird SB21 connected to the continuous system and surface solar radiation was measured by a radiometer located in the upper deck (model PRR-800) (PAR; W m⁻²).

2.2 Alkylamine sampling and analysis protocol

Seawater was collected into 50 mL propylene tubes (Falcon type), which were completely filled. For dissolved amine analysis, seawater was filtered through a 47 mm GF/F filter (0.7 µm pore size) by gravity (ca. 60 minutes, filtration timing depended on the microbial biomass and particulate matter contained in the sampled water) and directly collected into a new 50 mL propylene tube until completely filled. This procedure minimised headspace as indicated by Akenga and Fitzsimons (2024). This filtered water was preserved with concentrated 37 % HCl (analytical grade) at 1 % (v/v) final concentration. The tube was tightly closed and stored in the dark at 4 °C until analysis. In turn, after filtration, the GF/F filter was stored in a 2 mL eppendorf tube at -80 °C for particulate amine analysis.

2.2.1 Analysis of alkylamines in seawater by headspace-based solid-phase microextraction and gas chromatography with Nitrogen-Phosphorus detection

Dissolved and particulate amines in seawater were analysed following Akenga and Fitzsimons (2024). Briefly, the method comprises an online, automated headspace solid-phase microextraction step coupled with gas chromatography and nitrogen-phosphorus detection (HS-SPME-GC-NPD), optimising the method reported by Cree et al. (2018). The new protocol has improved precision, throughput and confidence with advantages in sample collection, storage and transport, particularly from remote environments (Fitzsimons et al., 2023). A sample chromatogram is shown in Fig. S1.

2.2.2 Reagents and labware

Methylamine standards, monomethylamine (MMA, 99 %), dimethylamine (DMA, 99 %), trimethylamine (TMA, 98 %) and diethylamine (DEA, 99 %) in hydrochloride form were purchased from Thermo Fisher, UK. Cyclopropylamine (CPA, 99 %), analytical grade HCl (37 %), 10 M NaOH and analytical grade NaCl were from Thermo Fisher, UK. All glassware was soaked for 24 h in Decon solution (2 %, v/v) and rinsed with high-purity water (HPW; 18.2 MΩ cm), then soaked in HCl (10 %, v/v) for 24h, rinsed again with HPW and allowed to dry at room temperature (RT).

2.2.3 Analysis of dissolved alkylamines

Dissolved amines, i.e., dMMA, dDMA, dTMA and dDEA stock standard solutions were prepared at 94.8, 59.4, 63.7 and 100 nM, respectively, after an accurate dissolution of their chloride salts in HPW. Stock solutions and working standards were acidified with concentrated HCl at a ratio of 1:1000 v/v (acid:solution). Calibration solutions for dMMA, dDMA and dTMA analyses were prepared in the ranges 9.48–94.8, 5.94–59.4 and 6.37–63.7 nM, respectively and at 10–100 nM for dDEA. Aliquots (10 mL) of the solutions were pipetted into 20 mL autosampler glass vials (cleaned as indicated above) then saturated with NaCl (33 %). CPA was used as an internal standard and was added to each vial at a final concentration of 20 nM. The pH of each standard solution was adjusted to > 13.0 through addition of 10 M NaOH solution (250 µL) and the vials were immediately sealed. At this point, alkylamines were converted to gaseous form and diffused into the headspace, where they were adsorbed into the SPME fibre. Blank samples were prepared with HPW and treated with NaCl and NaOH as described. Samples analyses were conducted ~6

months after collection. From each stored sample, three 10 mL aliquots were distributed in glass vials and treated analogously to the standards.

2.2.4 Analysis of particulate alkylamines

We also measured amines in particulates retained on GF/F filters after seawater filtration (section 2.2). Analyses were conducted ~6 months after sample collection. Prior to extraction, each filter was placed in a 20 mL autosampler glass vial and allowed to thaw inside the vial (one filter per vial). Subsequently, we added 250 μ L of CPA (20 nM final concentration) as internal standard and 500 μ L of 10 M NaOH, to liberate gaseous amines, and the vial was tightly sealed. This treatment was assumed to volatilize the target analytes into the vial headspace in a manner analogous to dissolved samples. Particulate amine concentrations were quantified using standard amine solutions, as described previously.

2.2.5 SPME and gas chromatography

Details of the automated method are provided in Akenga and Fitzsimons (2024). Briefly, the process involved extracting analytes onto an SPME fibre after equilibration in an integrated oven (60 °C), followed by injection of the SPME fibre into the GC (gas chromatography) system. Thermal desorption of the analytes occurred in the injector port (250 °C), followed by their separation and detection on a 60 m CP-Volamine column. Once separated, the analytes were detected by a nitrogen-phosphorus detector at 300 °C. The total run time lasted 25 minutes. Peak area data acquisition and processing was performed by ThermoChromeleon vs. 7.3 software. The three MAs and DEA were baseline resolved on the column and separated from CPA. The retention times of MMA, DMA, TMA, DEA and CPA were 7.2, 8.1, 8.6, 12.0 and 11.3 minutes, respectively (Fig. S1). An R^2 value >0.90 was achieved for the calibration of the four alkylamines. The limits of detection for MMA, DMA, TMA and DEA, were 9.5, 5.9, 1.1 and 4.3 nM, respectively. Additionally, the calibration curve for dissolved TMA was used to detect particulate TMA values.

2.3 Biological Parameters

2.3.1 Chlorophyll-a

Between 200 and 750 mL of seawater were filtered through 25 mm Whatman GF/F glass fibre filters to estimate the total chlorophyll-a concentration. All filters were stored at -20 °C until

analyses conducted on board the *R/V Hesperides*. Chlorophyll-a (Chl-a) concentrations were estimated fluorometrically after extraction in 90 % acetone at 4 °C for 24h (Yentsch and Menzel, 1963). Readings were conducted on a Turner 10AU fluorimeter calibrated with pure chlorophyll extract from spinach (Sigma C5357) using a Beckton-Dickinson spectrophotometer. A Carbon:Chlorophyll ratio of 50 (Jakobsen and Markager, 2016) was applied to estimate the phytoplankton biomass in terms of Carbon.

2.3.2 Viral and bacterial abundance and biomass

Subsamples (2 mL) were fixed with glutaraldehyde (0.5 % final concentration) for viruses, and with 1 % paraformaldehyde + 0.05 % glutaraldehyde for bacteria estimations by flow cytometry (FCM). After 15–30 min in the dark at 4 °C, the fixed samples were flash-frozen in liquid nitrogen and subsequently stored at -80 °C until analysis. Viral (Brussaard, 2004) and bacterial (Gasol and Del Giorgio, 2000) abundances were measured in a Cytoflex flow cytometer at the ICM-CSIC laboratory (up to 5 months after sampling). Samples for viral abundance were thawed and diluted with TE-buffer (10:1 mM Tris: EDTA), stained with 50x SYBR Green I to a final concentration of 1 %, heated in a 80 °C bath for 10 min and run at a constant flow rate of 60 $\mu\text{L min}^{-1}$ according to Brussaard (2004). Viruses were determined in bivariate scatter plots of the green fluorescence of stained nucleic acids *versus* side scatter. Based on their green fluorescent and side scatter signals, four distinct virus populations (V1–V4) were identified (Fig. S2). Presumably, V1 and V2 populations are dominated by bacteriophages (Biggs et al., 2021); the V3-V4 fractions by eukaryotic algal viruses (Evans et al., 2009), and V4 fraction correspond primarily to Haptophyceae (e.g., *Phaeocystis* spp.) viruses (Brussaard et al., 1999, 2005; Rocchi et al., 2022). Virus biomass was calculated using the carbon virus content factor of 0.2 fgC virus⁻¹ (Suttle, 2005). Thawed samples for bacterial abundance were stained with 50x SYBR Green I at a final 1 % concentration and incubated for 5 min in the dark. Based on the flow cytometer side scatter *versus* green fluorescence (FL1) signatures, high nucleic acid (HNA) from low nucleic acid (LNA) content bacteria were identified (Gasol and Del Giorgio, 2000) (Fig. S3). Bacterial biomass was obtained from the carbon-to-volume relationship (Norland, 1993) namely, $\text{pgC cell}^{-1} = 0.12 \times (\text{V})^{0.7}$, where V is the bacteria volume cells in μm^3 . Here, an average cell volume of 0.066 μm^3 bacteria⁻¹ reported for Antarctic waters (Vaqué et al., 2004) was used.

2.3.3 Pico- and nanophytoplankton abundance and biomass

Samples for photosynthetic pico- and nanophytoplankton abundances were collected on 5 mL cryovials, fixed with glutaraldehyde (1% final concentration) and frozen in liquid nitrogen following Vaultot et al. (1989). Cells were counted by a CyFlow Cube 8 flow cytometer (Sysmex) at the ICM-CSIC. Phytoplankton cells were detected with a 488 nm laser beam from their signatures in a plot of side scatter (SSC) *versus* red fluorescence (FL3), separating the picophytoplankton size class of 1–2 μm (sphere equivalent diameter, SED), and the nanophytoplankton size classes with SEDs of 2–7 μm , 7–15 μm , and 15–20 μm (Fig. S4). Within the nanophytoplankton, Cryptophytes (*Cryptomonas* spp.) were identified by their phycoerythrin signal in the FL3 vs orange fluorescence (FL2) plots (Marie et al., 2014). Biomasses ($\mu\text{g C L}^{-1}$) of these cell sizes were measured using the formula, $\text{pgC cell}^{-1} = 0.216 \times (V)^{0.939}$ (V, cell volume; Menden-Deuer and Lessard, 2000). The phytoplankton cell volume varied between 1.8 and 63 $\mu\text{m}^3 \text{ cell}^{-1}$.

2.3.4 Nanoflagellate abundance and biomass

Abundances of heterotrophic and phototrophic nanoflagellates, including *Phaeocystis*, in the size fraction 2–20 μm (SED) were determined by epifluorescence microscopy. 30 mL seawater samples were fixed with glutaraldehyde (1 % final concentration), filtered through 0.6 μm black (25 mm diameter) polycarbonate filters, and stained with 4,6-diamidino-2-phenylindole (DAPI) at a final concentration of 5 $\mu\text{g mL}^{-1}$ (Sieracki et al., 1985). Filters were placed on slides and kept frozen (-20 °C). Microscope cell counts of heterotrophic (HNF) and phototrophic nanoflagellates (PNF) were estimated by the fluorescence response of the cells after blue light illumination using an Olympus BX40-102/E at 1000X epifluorescence microscope. PNFs were distinguished by red fluorescence emitted by photosynthetic plastid structures, while HNF were identified from the yellow fluorescence of DAPI stained nuclei. At least 50 HNFs and 50 PNFs were counted per sample (3 transects of 5 mm in each filter) and classified into $\leq 2 \mu\text{m}$, 2–5 μm , 5–10 μm , and 10–20 μm size (SED) classes. The nanoflagellate carbon cell content was estimated from the corresponding carbon-to-volume ratio, e.g., $\text{pgC cell}^{-1} = 0.216 \times (V)^{0.939}$ (Menden-Deuer and Lessard, 2000), where the cell volume (V) was calculated from the average length of each nanoflagellate cell size class and transformed into spherical or ellipsoidal volume. The nanoflagellate cell volume varied between 1.8 and 57.6 $\mu\text{m}^3 \text{ cell}^{-1}$.

2.3.5 Microplankton assemblages

The microplankton community was characterised using the Utermöhl method on 125 mL neutral lugol fixed seawater samples. 50 mL aliquots samples were settled in sedimentation chambers for 24 h and observed in a Leica MDi1 inverted microscope (Edler and Elbrächter, 2010). The identified taxa and size classes included: dinoflagellates (resting cysts, vegetative dinoflagellates 10–20 μm , 20–40 μm , and $> 40 \mu\text{m}$), diatoms (10–20 μm , 20–40 μm , and $> 40 \mu\text{m}$) and ciliates. When possible, taxa were identified at the genus and species level. The relative biomasses (in $\mu\text{gC L}^{-1}$) were measured from cell volumes using the carbon-to-volume relationships estimated by Menden-Deuer and Lessard (2000) on diatoms and dinoflagellates. Namely, the equation $\text{pgC cell}^{-1} = 0.760 \times (\mu\text{m}^3 \text{ cell}^{-1})^{0.819}$ was used for dinoflagellates and $\text{pgC cell}^{-1} = 0.288 \times (\mu\text{m}^3 \text{ cell}^{-1})^{0.811}$ for diatoms. The biovolume was estimated considering an ovoid, cylinder or prism shape for dinoflagellates, centric diatoms, and pennate diatoms, respectively, and empty sphere for empty dinoflagellate cysts. Cell dimensions measurements (excluding chaetae and other cell expansions) were conducted using a digital camera and specific calibration of the used Leica DMi1 microscope. Empty diatom frustules were assumed to have a null contribution to C.

2.3.6 Photosynthetic efficiency

The relative efficiency of excitation energy captured by the photosystem II (PSII), calculated as F_v'/F_m' , is used as a proxy of phytoplankton stress and fitness (Gorbunov et al., 2020; Gorbunov and Falkowski, 2022). The metric is measured by a multi-color fluorescence induction and relaxation instrument (mini-FIRE system) (Gorbunov et al., 2020). The instrument records two parameters: F_0' as the minimal yield of fluorescence before fast light flashes, and F_m' , the maximum yield of fluorescence due to the reradiation of the maximum number of photons. The difference between F_m' and F_0' is called variable fluorescence (F_v'). The quotient of F_v'/F_m' represents the effective photosynthetic efficiency of the community measured under light conditions (Gorbunov and Falkowski, 2022). F_v'/F_m' has no units, so that it is independent of the phytoplankton abundance and allows comparisons between environments. Aliquots of 10 mL were sampled from the underway system and rapidly placed in the chamber of the mini-FIRE to apply the induction and relaxation protocol for dilute samples. No dark acclimation period was used.

2.4 Chemical parameters

2.4.1 Particulate Organic Carbon and Nitrogen

Particulate organic carbon (POC) and nitrogen (PON) content in the seawater was determined by filtration of 390 to 1000 mL through pre combusted (450 °C, 4h) 25mm GF/F glass fibre filters (Whatman) at low pressure (<20mmHg) and kept frozen (-80 °C) until analysis. Filters were thawed and dried at RT, exposed to 37 % (pure) HCl atmosphere in a hermetic beaker to eliminate carbonate salts and subsequently analysed with an Elemental Analyser (Perkin-Elmer 2400 CHN) at the Scientific and Technical Service of the University of Barcelona. In the following, the term POC and PON will refer to the C and N estimated biochemically as described here as a proxy of particulate organic matter, consisting in living and non-living cells, extracellular material and detritus containing C or N.

2.4.2 Dissolved Carbon and Nitrogen

For total organic carbon (TOC) and nitrogen (TN: organic and inorganic nitrogen) analyses, 30 mL of seawater was filtered through a HCl clean 200 µm mesh by gravity and collected in polycarbonate bottles. The sample was fixed with 100 µl of 25 % H₃PO₄ stored frozen (-20 °C) until analysis in the laboratory. Following the elimination of inorganic C (i.e., carbonates) by the acidification of the sample, determination of TOC and TN in seawater was conducted by high temperature catalytic oxidation (680 °C and 720 °C, respectively) as described in Álvarez-Salgado and Miller (1998). Measurements were conducted with the TOC-L Shimadzu autoanalyzer, with deep Sargasso Sea water used as control (Hansell Laboratory, University of Miami, RSMAS). Concentrations are expressed as µM (µmol C L⁻¹ or µmol N L⁻¹). Dissolved Organic Carbon (DOC) and Nitrogen (DON) were calculated by subtraction of POC from TOC, and nitrate, nitrite, ammonium and PON concentrations from TN, respectively.

2.4.3 Dissolved inorganic nutrient analysis and total Phosphorus

For measurements of nutrient concentrations, seawater samples were collected in two different 50 mL polypropylene plastic tubes: one tube was used for the determination of inorganic nutrients (nitrate, nitrite, ammonium, phosphate and silicate) and the other one for total phosphorus (TP, organic and inorganic forms). Samples were immediately frozen and stored at -20 °C until analysis. Concentrations of inorganic nutrients were determined with an AA3 HR autoanalyzer (Seal

Analytical) and TP with an AA3 autoanalyzer after previous digestion, following Grasshoff et al. (1983).

2.4.4 Total dimethylsulfoniopropionate (DMSP) concentrations

Samples for total DMSP (DMSPt) analysis were collected directly from the underway system on ~30 mL borosilicate serum vials and processed following Kinsey and Kieber (2016). The vials were uncapped and individually heated by microwave until they began to boil. After the first bubble formed, the microwave was stopped and the vial was left to cool. Subsequently, 30 µl of 37 % HCl were added to all the vials to remove the DMS present and preserve the DMSP. Acidified samples were stored at RT in the dark. Within six months of the cruise, DMSP was converted to DMS by alkaline hydrolysis with NaOH for at least 24 hours. The resulting DMS was quantified with a cryogenic purge-and-trap system coupled to a Thermo Fisher TRACE 1300 gas chromatograph with flame photometric detection following Masdeu-Navarro et al. (2022).

2.4.5 DMS measurements by Proton Transfer Reaction Time-of-Flight Mass Spectrometry (PTR-ToF-MS)

A Vocus-PTR-ToF-MS coupled to a segmented flow coil equilibrator was used to continuously measure seawater dissolved DMS (Wohl et al., 2019). An overview on operation and calibrations is provided in Wohl et al. (2024).

2.5 Statistical analyses

All analyses were conducted in the RStudio integrated development environment (RStudio Team, 2023) to ensure reproducibility and clarity. Multivariate statistical analyses were performed using R version 4.3.2 (R Core Team, 2023) to explore relationships among variables. The data were normalised by centering and scaling to ensure equal contribution of all variables to the Principal Component Analysis (PCA). The PCA was conducted to reduce dimensionality and examine the relationships among variables. The analysis employed the princomp() function from the stats package (Bolar, 2019), using the correlation matrix of normalized data as input to focus on inter-variable relationships. Visualizations were generated using the factoextra package version 1.0.7 (Kassambara and Mundt, 2020). The ggcorrplot package (Kassambara, 2021) was used to create a heatmap of variable correlations, while the gridExtra package (Auguie, 2017) facilitated side-by-

side comparisons of variable contributions to principal components. Factor Analysis was performed to uncover latent structures within the dataset using the psych package version 2.3.6 (Revelle, 2023). Factor extraction employed Principal Axis Factoring with Varimax rotation to achieve interpretability, complemented by Maximum Likelihood Estimation for comparison. Factor loadings were visualized using ggplot2 version 3.4.4 (Wickham, 2023). Mantel Test was used to assess the correlation between two distance matrices using the vegan package version 2.6-4 (Oksanen, 2022). For each pair of variables, Euclidean distance matrices were computed and tested for significant Pearson correlations. Results with p-values < 0.05 were considered significant. The Wilcoxon test and ggplot2 were used to analyze and visualize statistical differences between the Antarctic Peninsula and Weddell Sea groups, with a logarithmic y-axis improving data interpretation.

3 Results

3.1 Cruise setting

The regional satellite images of SST and Chlorophyll concentration during the cruise period (Fig. 1) indicates two distinct areas where the PolarChange cruise was conducted: the Western Antarctic Peninsula and the northern Weddell Sea. For this reason, in the following we will explore potential differences between these two areas concerning biological and biochemical parameters (Fig. S5). Sea surface temperature (SST) ranged between -0.7 and 2.4 °C (Table S1) with statistical differences within the two studied marine areas, (average \pm SD values) 1.9 ± 0.6 °C (n=7) in the western part of the Antarctic Peninsula compared to the colder waters of the Weddell Sea with 0.2 ± 0.7 °C (n=12; p=0.0072) (Table S1 and Fig. S5). Salinity (Table S1) remained relatively constant throughout the expedition, averaging 33.9 ± 0.3 . Concerning solar irradiance (Table S1), higher but not significantly different values were observed near the Antarctic Peninsula, 355 ± 257 W m⁻², compared to the 226 ± 194 W m⁻² numbers observed in the Weddell Sea.

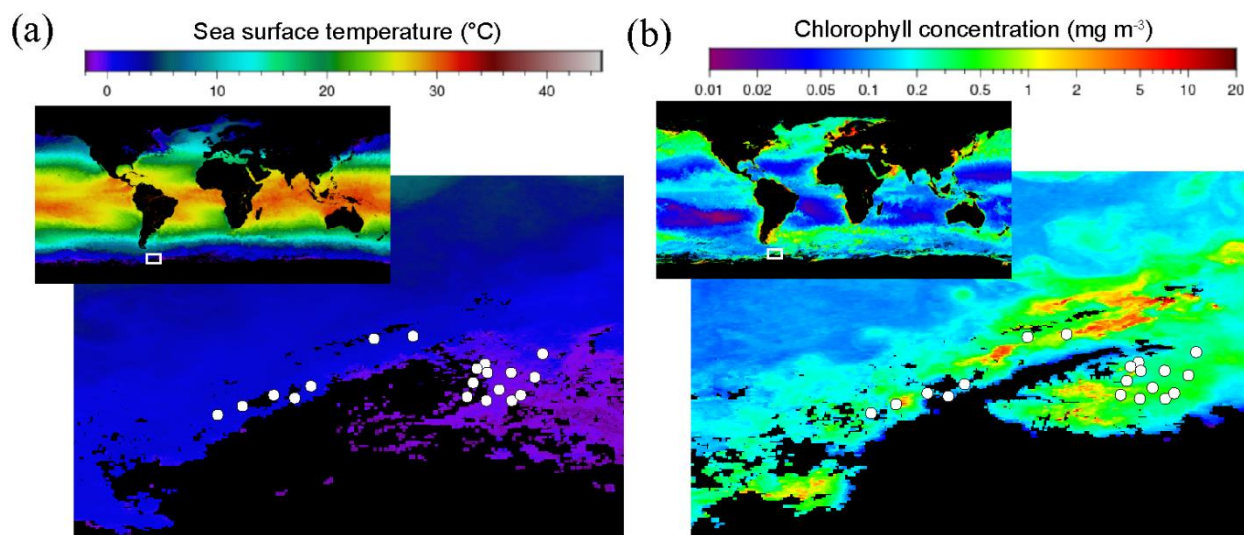


Figure 1. Satellite images of (a) the sea surface temperature and (b) the chlorophyll distribution in the ocean (small upper insert) with a zoom in the Southern Ocean around the Antarctic Peninsula and the Weddell Sea in March 2023 during the period of the PolarChange cruise when most amine samples were collected. White circles indicate the location of the 19 stations where all samples analysed in this study were collected (the first seven stations are located in the Western Antarctic Peninsula, while the remaining twelve stations are situated in the Weddell Sea; see stations list in Table S1). Chlorophyll concentration is estimated from the Ocean Color Index (OCI) Algorithm and the sea surface temperature from SNPP VIIRS satellite, <https://oceancolor.gsfc.nasa.gov/13/>.

3.2 Alkylamine concentrations

3.2.1 Dissolved alkylamines

We detected dissolved MAs and DEA at ~4 m of depth over the cruise (Fig. 2a and Table S1). Dissolved MMA (dMMA) was quantitatively identified only in samples #9, #10, #11 in the Weddell Sea with an overall concentration average of 12.7 ± 0.1 nM ($n=3$). With this method we could detect dDMA in most of the samples, ranging from 7.6 nM to 132.3 nM with an average of 32.3 ± 32.7 nM ($n=15$); it was below detection limits in samples #12, #14, #15, #16. The concentration of dDMA was statistically higher near the Antarctic Peninsula compared to the Weddell Sea (respectively, 49.9 ± 39.6 nM, $n=7$ and 17.0 ± 11.4 nM, $n=8$; $p=0.04$) (Fig. S5). dTMA was measured in all the samples varying from 1.5 nM to 67.9 nM with an average of 20.9 ± 15.2 nM ($n=19$) (20.8 ± 10.6 nM, $n=7$ for the Western Antarctic Peninsula and 21.0 ± 17.3 nM, $n=12$ for the Weddell Sea; $p=0.77$). dDEA was identified in all the samples but with lower concentrations than the dissolved MAs along the studied area (Table S1). dDEA concentrations ranged between 5.1 nM and 13.3 nM, with an average of 7.2 ± 1.7 nM ($n=19$) (7.7 ± 2.5 nM, $n=7$

for the Western Antarctic Peninsula and 6.9 ± 1.0 nM, n=12 for the Weddell Sea; p=0.77). In this study, dDEA had the most even distribution of all alkylamines (excluding dMMA), with a coefficient of variation of 23 %, compared to 101 % for dDMA and 73 % for dTMA.

3.2.2 Particulate alkylamines

Only pTMA was detected and identified (Fig. 2b and Table S1) in 18 filter samples (sample #3 was lost), i.e., associated with particles. pTMA showed concentrations ranging between 9.7 nM and 28.1 nM with an average of 14.4 ± 4.6 nM (14.5 ± 6.2 nM, n=6 for the Western Antarctic Peninsula and 14.4 ± 3.6 nM, n=12 for the Weddell Sea; p=0.62).

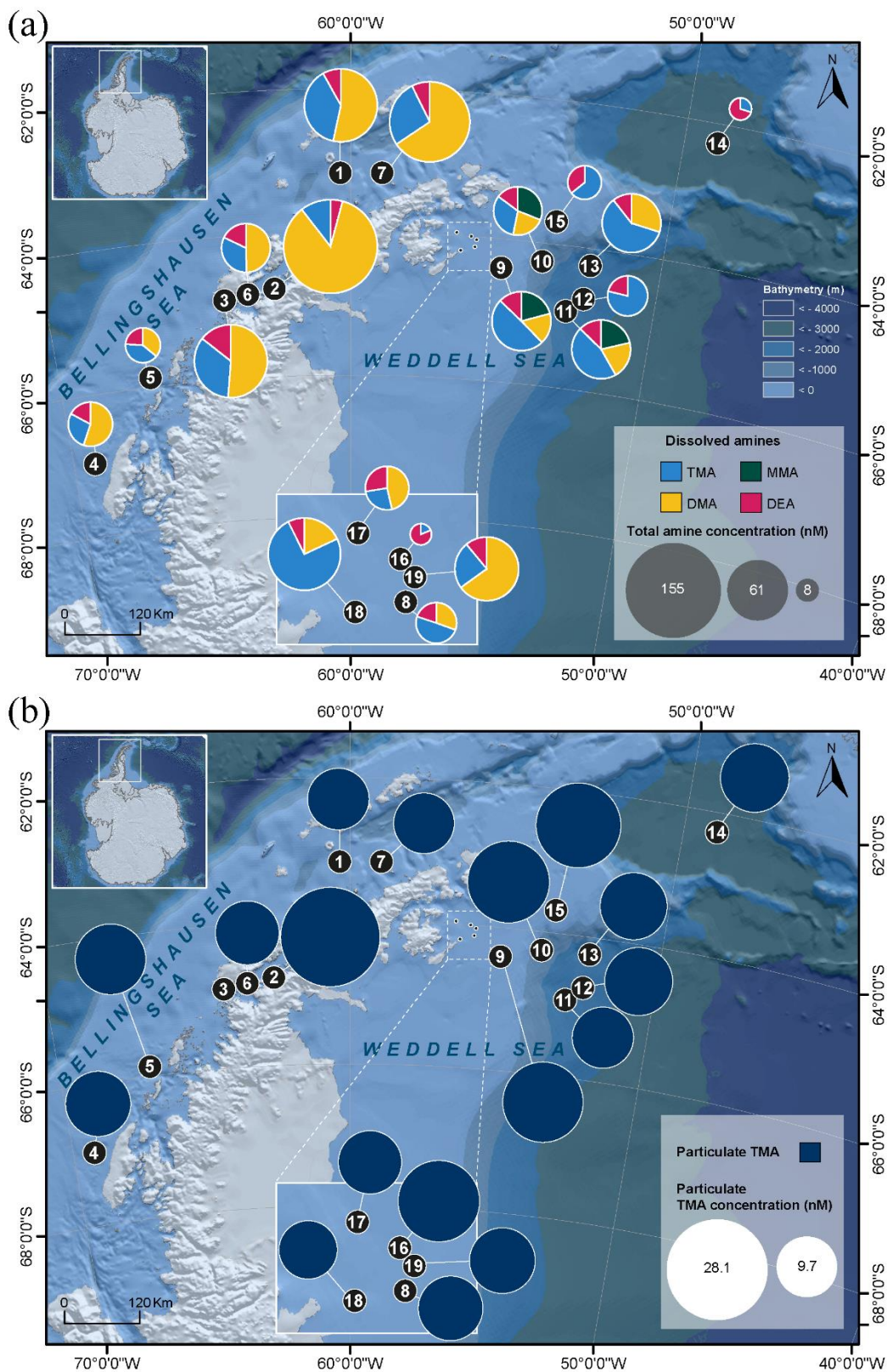


Figure 2. Distribution of the concentrations (using pie charts) of (a) the four dissolved alkylamines (MMA, DMA, TMA and DEA) and (b) particulate TMA (*note that the particulate sample #3 was lost) in the studied area.

3.3 Biological variables

3.3.1 Chlorophyll-a concentrations

The Chl-a concentrations varied along the oceanographic cruise, from 0.2 to 9.6 $\mu\text{g L}^{-1}$, throughout the area (Fig. 1), with an average of $1.2 \pm 2.0 \mu\text{g L}^{-1}$ (n=19) (Table S2). More productive waters were found in the western side of the Antarctic Peninsula, with an average of $2.5 \pm 2.9 \mu\text{g L}^{-1}$ (n=7) significantly higher than the values observed in the Weddell Sea samples ($0.5 \pm 0.3 \mu\text{g L}^{-1}$, n=12; p=0.0077) (Fig. S5).

3.3.2 Viral and bacterial abundances

Viral abundances (VA) (Table S2) averaged $8.2 \pm 3.8 \times 10^6$ viruses mL^{-1} (n=19) and the V1, V2 and V3 populations accounted, on average and respectively, for the 80 %, 16.5 % and 3.5 % of total VA. V4 was only present in sample #15 with an abundance of 1.8×10^5 viruses mL^{-1} . On average, total VA was significantly higher near the Antarctic Peninsula ($11.5 \pm 3.8 \times 10^6$ viruses mL^{-1} , n=7) than in the Weddell Sea ($6.2 \pm 1.9 \times 10^6$ viruses mL^{-1} , n=12; p=0.013) (Table S2 and Fig. S5). V1 abundance was also significantly higher in the Antarctic Peninsula ($9.4 \pm 3.1 \times 10^6$ viruses mL^{-1} , n=7) than in the Weddell Sea ($4.9 \pm 1.7 \times 10^6$ viruses mL^{-1} , n=12; p=0.0098) (Table S2 and Fig. S5). Concerning bacterial abundances (BA), the total average was $6.4 \pm 2.5 \times 10^5$ cells mL^{-1} (n=19) with slightly (but not significantly different) higher numbers in the waters near the Antarctic Peninsula ($7.0 \pm 1.6 \times 10^5$ cells mL^{-1} , n=7) compared to Weddell Sea ($6.0 \pm 2.8 \times 10^5$ cells mL^{-1} , n=12). However, the highest value was estimated in sample #16 (11.7×10^5 cells mL^{-1}) (Table S2) collected in the Weddell Sea. Generally, most bacteria had a high nucleic acid content, indicating that more than half of the total bacteria numbers were active cells (Table S2). Note that here, we are referring to cell abundances and not to biomass; C concentration values calculated from cell numbers followed the same patterns as cell abundances for each microorganism described (data not shown in the text, see SI).

3.3.3 Pico- and nanophytoplankton abundances

Regarding phytoplankton measured by FCM, the abundances of the five identified groups (1–2 μm , 2–7 μm , 7–15 μm , 15–20 μm and Cryptophytes) were $1.6 \pm 1.7 \times 10^3$, $1.8 \pm 0.6 \times 10^3$, $5.7 \pm 7.5 \times 10^2$, $1.3 \pm 2.5 \times 10^2$, $1.5 \pm 2.5 \times 10^2$ cells mL^{-1} , respectively (average \pm SD values, n=19; Table S2). Picophytoplankton cells, ranging from 1 to 2 μm in size, exhibited significantly higher

abundances around the Antarctic Peninsula, with an average of $3.3 \pm 1.8 \times 10^3$ cells mL⁻¹ (n=7), compared to the Weddell Sea ($6.1 \pm 4.1 \times 10^2$ cells mL⁻¹, n=12; p<0.001) (Fig. S5). Conversely, the average abundance of the larger cells, nanophytoplankton, ranging from 2 to 20 µm, appeared marginally higher in the Weddell Sea ($2.7 \pm 0.9 \times 10^3$ cells mL⁻¹, n=12) than in the western part of the Antarctic Peninsula ($2.2 \pm 1.5 \times 10^3$ cells mL⁻¹, n=7). Specifically, the abundance of nanophytoplankton cells 2–7 µm in size was significantly greater in the Weddell Sea compared to the Antarctic Peninsula coasts (2.1 ± 0.5 and $1.3 \pm 0.5 \times 10^3$ cells mL⁻¹, n=19; p=0.0072) (Fig. S5). Similarly, cryptophytes (*Cryptomonas* spp.) presented abundances of 112 ± 143 cells mL⁻¹ (n=7) in the Western Antarctic Peninsula in contrast to 146 ± 121 cells mL⁻¹ (n=12) in the Weddell Sea.

3.3.4 Nanoflagellate abundances

Abundances of HNF and PNF measured by epifluorescence microscopy were, on average, of 986 ± 951 cells mL⁻¹ and 5046 ± 2538 cells mL⁻¹ (n=15; samples #5, #9, #11 and #15 were lost), respectively (Fig. 3 and Table S3). In the Western Antarctic Peninsula, the abundances were 1234 ± 1195 cells mL⁻¹ for HNF and 4240 ± 1688 cells mL⁻¹ for PNF (n=6). In comparison, in the Weddell Sea, the abundances were 820 ± 698 cells mL⁻¹ for HNF and 5583 ± 2849 cells mL⁻¹ (n=9) for PNF. Concerning size, in the case of HNF, the 2 to 5 µm group, constitutes the largest proportion of total abundance followed by the smallest size category (≤ 2 µm), the 5 to 10 µm group, and finally, the largest category ranging from 10 to 20 µm. Similarly, for PNF, the smallest size categories (≤ 2 µm and 2–5 µm) were the most abundant, followed by the 5–10 µm category, and lastly, the largest category spanning 10 to 20 µm (Table S3). PNF 5–10 µm showed a statistical difference between the two Antarctic areas with barely higher concentrations in the Weddell Sea (117.3 ± 88.3 and 193.6 ± 74.4 cells mL⁻¹, n=15; p=0.045) (Fig. S5). Total PNF exhibited slightly greater abundances in the Weddell Sea. Additionally, *Phaeocystis* presented slightly lower abundances west of the Antarctic peninsula of 208 ± 169 cells mL⁻¹ (n=6) in contrast to 352 ± 383 cells mL⁻¹ (n=9) in the Weddell Sea (Table S3).

3.3.5 Composition and abundance of microplankton assemblages

A diverse range of phytoplankton taxa was found in the studied period in the Antarctic marine environments (Fig. 3 and Table S4). In the smallest size of the dinoflagellate group (10–20 µm), the identified taxa were *Gymnodinium* spp., Kareniaceae, *Oxytoxum* spp. and *Prorocentrum cordatum* (= *P. minimum*). The intermediate size group (20–40 µm) included larger taxa such as

458 *Gymnodinium* spp., *Protoperidinium bipes*, *Gyrodinium* spp., Kareniaceae cells, and
 459 *Lebouridinium glaucum* (= *Katodinium glaucum*). In the >40 µm category, only *Gyrodinium* spp.
 460 and *Gymnodinium* spp. heterotrophs were present. Among diatoms, in the 10–20 µm size group,
 461 we identified a variety of genera, including centric and pennate chains, *Thalassiosira*, *Porosira*,
 462 *Coscinodiscus*, *Fragilaria*, *Chaetoceros* and *Amphora*. In the 20–40 µm size range, larger cells of
 463 *Coscinodiscus*, *Corethron criophilum* and its spores, pennate chains like *Pseudo-nitzschia*,
 464 *Proboscia alata*, *Licmophora*, *Achnanthes*, *Navicula*, *Leptocylindrus*, and *Actinocyclus* were
 465 observed. Among the larger diatoms (>40 µm), we identified *Coscinodiscus*, *Corethron*
 466 *criophilum*, and *Chaetoceros* spp., *Proboscia alata*, *Lioloma* chains, *Rhizosolenia curvata*,
 467 *Actinocyclus* and pennate diatoms. Non-photosynthetic taxa included mainly tintinnid ciliates.

468 Dinoflagellates were particularly dominant, though in general, they were distributed close to the
 469 Antarctic Peninsula. Specifically, dinoflagellate cysts accounted for ca. $1.2 \pm 1.1 \times 10^3$ cells L⁻¹
 470 (n=7), compared to $0.8 \pm 1.6 \times 10^3$ cells L⁻¹ in the samples from the Weddell Sea (n=12).
 471 Dinoflagellates 10–20 µm were found at concentrations of $6.9 \pm 5.8 \times 10^3$ cells L⁻¹ (n=7) near the
 472 Antarctic Peninsula, compared to $1.3 \pm 1.2 \times 10^4$ cells L⁻¹ (n=12) in the Weddell Sea. Intermediate-
 473 sized dinoflagellates (20–40 µm) had similar abundances in both seas, with $9.7 \pm 5.1 \times 10^3$ cells
 474 L⁻¹ in the Antarctic Peninsula waters (n=7) and $1.7 \pm 2.3 \times 10^4$ cells L⁻¹ in the Weddell Sea (n=12).
 475 Larger dinoflagellates (>40 µm) were more concentrated in the Antarctic Peninsula waters, with
 476 $1.2 \pm 1.4 \times 10^3$ cells L⁻¹ (n=7) compared to $3.2 \pm 4.9 \times 10^2$ cells L⁻¹ (n=12) in the Weddell Sea.
 477 Similarly, diatoms were more abundant near the Antarctic Peninsula waters: smaller diatom cells
 478 (10–20 µm) were significantly more prevalent in this area ($2.0 \pm 3.7 \times 10^5$ cells L⁻¹, n=7) compared
 479 to the Weddell Sea ($4.7 \pm 9.1 \times 10^5$ cells L⁻¹, n=12; p=0.0087) (Fig. S5). Furthermore, sample #1
 480 exhibited the highest abundance of diatoms within the 10–40 µm size range compared to all other
 481 samples (Fig. 3). Intermediate-sized diatoms followed a similar pattern, with $1.2 \pm 2.9 \times 10^5$ cells
 482 L⁻¹ (n=7) near the Antarctic Peninsula waters and $6.7 \pm 8.5 \times 10^2$ cells L⁻¹ (n=12) in the Weddell
 483 Sea. Larger diatoms (>40 µm) presented significantly higher concentrations ($3.5 \pm 2.9 \times 10^3$ cells
 484 L⁻¹, n=7) in the Antarctic Peninsula area than ($8.0 \pm 5.8 \times 10^2$ cells L⁻¹, n=12; p=0.028) in the
 485 Weddell Sea (Fig. S5). In contrast, ciliates showed slightly higher abundances in the Weddell Sea,
 486 averaging $4.5 \pm 8.2 \times 10^2$ cells L⁻¹ (n=12) compared to $4.1 \pm 3.5 \times 10^1$ cells L⁻¹ (n=7) in the Western
 487 Antarctic Peninsula.

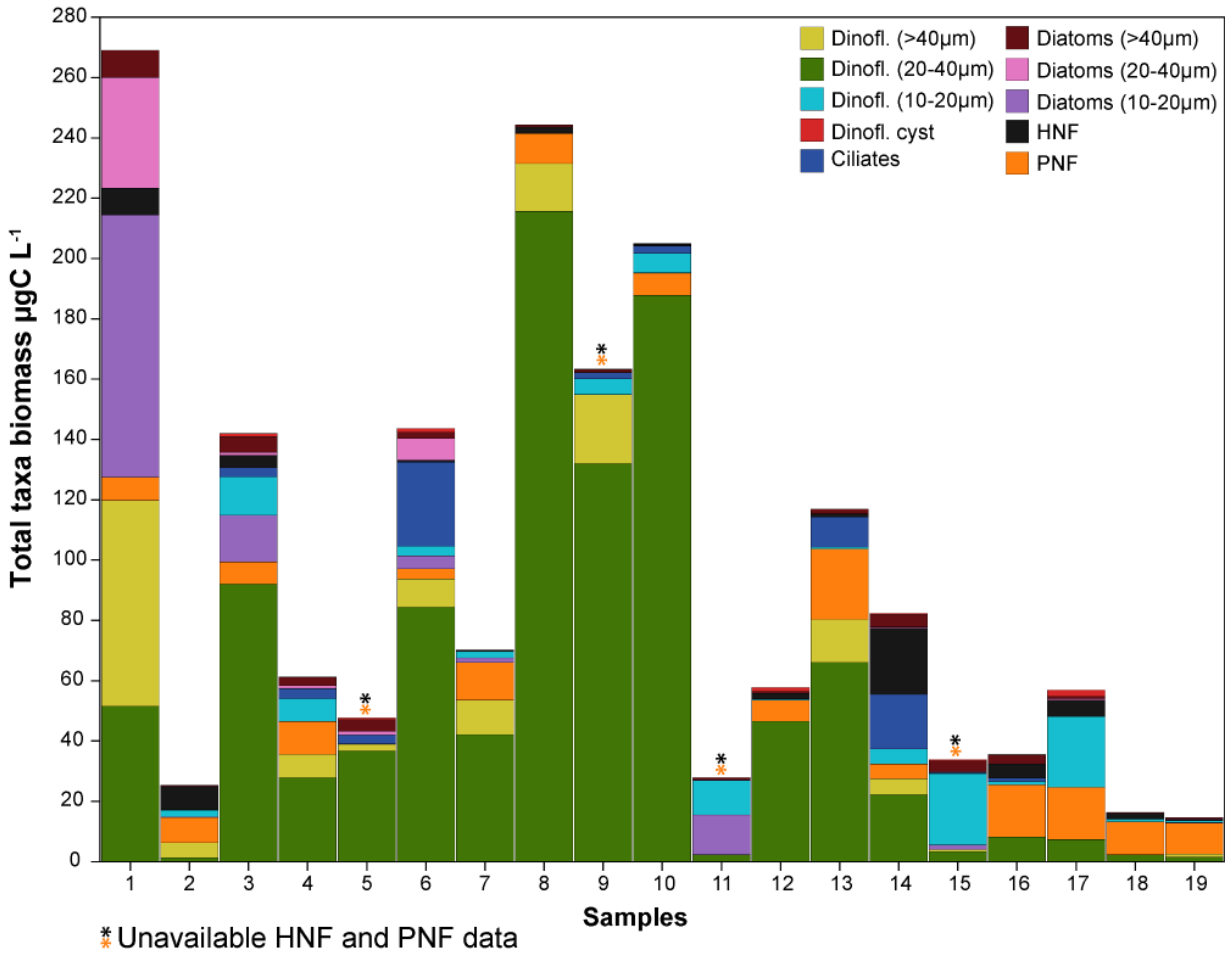


Figure 3. Biomass (µg C L⁻¹) and proportions (represented by the barplots) of the main phytoplankton groups, protist and microzooplankton in the 19 samples obtained in the studied area (*note that samples #5, #9, #11, #15 of HNF and PNF were lost).

3.3.6. Photosynthetic efficiency (F_v'/F_m')

The ecophysiological state and fitness of phytoplankton (F_v'/F_m') ranged between 0.21 and 0.54, with an average of 0.38 ± 0.10 (n=19). Values were slightly yet not significantly higher in the samples near the Antarctic Peninsula (0.41 ± 0.06 , n=7) compared to the samples collected in the Weddell Sea (0.36 ± 0.11 , n=12; p=0.36).

3.4 Chemical variables

3.4.1 Organic Carbon and Nitrogen

DOC and DON averaged $62.5 \pm 32.5 \mu\text{M}$ ($n=19$) and $6.1 \pm 3.1 \mu\text{M}$ ($n=15$), respectively, during this expedition (Table S5). Note that DON was below detection limit in 4 samples. Differences were observed between the two polar regions. Near the Antarctic Peninsula, DOC exhibited a lower concentration, $57.6 \pm 7.4 \mu\text{M}$ ($n=7$), in contrast to the Weddell Sea, with slightly higher DOC levels ($77.4 \pm 36.8 \mu\text{M}$, $n=12$) (Table S5). Similarly, TN and DON concentrations were slightly higher in the Weddell Sea, measuring $29.1 \pm 5.8 \mu\text{M}$ ($n=12$) and $6.3 \pm 4.1 \mu\text{M}$ ($n=10$), respectively, compared to the Western Antarctic Peninsula, where concentrations of $27.4 \pm 2.4 \mu\text{M}$ ($n=7$) and $5.3 \pm 2.9 \mu\text{M}$ ($n=5$) were measured. The average contribution of dissolved amines (dMMA, dDMA, dTMA and dDEA) to DOC and DON was determined to be $0.3 \pm 0.2 \%$ ($n=19$) and $1.8 \pm 2.8 \%$ ($n=15$), respectively.

POC and PON were measured in all samples, with averages of $7.6 \pm 5.3 \mu\text{M}$ ($n=19$) and $1.2 \pm 0.9 \mu\text{M}$ ($n=19$), respectively (Table S5). Statistical analysis revealed significantly higher POC and PON concentrations in the Western Antarctic Peninsula (POC: $10.7 \pm 7.3 \mu\text{M}$, PON: $1.8 \pm 1.2 \mu\text{M}$, $n = 7$) than in the Weddell Sea (POC: $5.7 \pm 1.7 \mu\text{M}$, PON: $0.9 \pm 0.2 \mu\text{M}$, $n = 12$) ($p=0.036$ for POC and $p=0.028$ for PON) (Fig. S5). C:N ratio of POM closely approximated the canonical Redfield ratio of 6.6, with an observed mean of 6.4 ± 0.6 ($n=19$) (Table S5). The contribution of particulate TMA to POC and PON averaged $0.7 \pm 0.3 \%$ and $1.5 \pm 0.6 \%$ ($n=18$ for both), respectively.

3.4.2 Sulfur compounds

DMSP concentrations averaged $35.1 \pm 16.6 \text{ nM}$ considering all samples ($n=19$) (Table S5). A disparity in the concentration of this sulfur compound was observed between the Western region of the Antarctic Peninsula and the Weddell Sea, where concentrations averaged $44.8 \pm 20.9 \text{ nM}$ ($n=7$) and $29.4 \pm 9.8 \text{ nM}$ ($n=12$), respectively. Similarly, DMS, the breakdown product of DMSP, showed statistically significant differences between samples, with higher values at the Western Antarctic Peninsula ($1.7 \pm 0.4 \text{ nM}$, $n=7$) and lower values in the Weddell Sea ($1.0 \pm 0.4 \text{ nM}$, $n=12$; $p=0.011$) (Table S5 and Fig. S5).

3.4.3 Nutrients

Nutrient levels remained relatively stable throughout the duration of the cruise, with average concentrations of 21.0 ± 2.5 , $0.2 \pm 0.0 \mu\text{M}$ for Nitrate, Nitrite, and $54.9 \pm 6.1 \mu\text{M}$ for Silicate, respectively ($n=19$) (Table S5). Contrastingly, Ammonium, Phosphate and TP showed statistically

significant differences within the two marine areas with higher values for Weddell Sea, 1.6 ± 0.4 μM for Ammonium, 2.3 ± 0.2 μM for Phosphate and 17.5 ± 9.0 μM for TP compared to the Western Antarctic Peninsula area, 0.8 ± 0.2 ($n=19$; $p<0.001$), 1.9 ± 0.3 ($n=19$; $p=0.0098$) and 4.9 ± 1.9 μM ($n=19$; $p=0.0018$).

3.5 Multivariate statistical analysis of the distributions of alkylamines, microbiota, chemical and environmental variables

We investigated how seawater biogeochemistry influences amine concentrations to address the largely unexplored role of microbiology and ecology in marine alkylamine cycles. Principal Component Analyses were conducted to examine correlations among a suite of physical, biogeochemical (including amine forms) variables and biomass data for microbial and viral populations of the 18 sampled stations (sample #3 was excluded because pTMA was missing) (Fig. 4). Variables like dMMA, DON, V4 and nanoflagellate biomasses were excluded from the PCA analyses because they were not detected in all samples, dinoflagellates and diatoms 10–20 μm biomass, TN, TOC and TON were excluded because they overlapped with included variables. Overall, the distribution of variable vectors within the multidimensional space of the PCA should help understand how environmental and biological variables influence the variability of marine alkylamines.

The first PCA, PCA (a), (Fig. 4a) provided an integrative perspective on the microbial community structure, encompassing the biomass of total bacteria, virus, phytoplankton biomasses (phytoplankton > 1 μm , including cryptophytes quantified by flow cytometry; and dinoflagellates cysts, dinoflagellates and diatoms >20 μm biomass, determined by optical microscopy) and biomass estimates for ciliates, assessed via optical microscopy. Additionally, it included physical (SST, salinity, PAR) and biogeochemical (DMSP, DMS, Chlorophyll-a, F_v'/F_m' , POC, PON, DOC, TP and nutrients) variables. The first two principal components (PC1 and PC2) accounted for 57.4 % and 14.9 % of the total variance, respectively. In PCA (a), while abiotic factors (SST, ammonium, phosphate), particulate organic matter (POC, PON) and total virus biomass were the most significant contributors to PC1, pTMA, dDMA, DMSP, Nitrate and Silicate contributed predominantly in a positive direction to the PC2 axis (Fig. 4a). The observed methylamines were neither aligned with physical parameters, nor with phytoplankton biomass or chlorophyll-a, which may be regulated by e.g. iron (Fe) availability (not measured in this study). However, they more

strongly covaried with nutrient concentrations, particularly silicate, and DMSP. Note that the expedition took place during a transitional period, after the peak of the ice melt and associated diatom blooms, alongside the initial stages of sea-ice formation.

Figure 4b further delves into a second analysis, PCA (b), focusing on specific biomass categories, including phytoplankton 1–2 μm , phytoplankton 2–20 μm (containing cryptophytes), diatoms 20–40 μm and >40 μm , dinoflagellates 20–40 μm and >40 μm , V1, V2 and V3 viral fractions, and HNA and LNA bacteria, each of them characterized by optical microscopy or FCM. This detailed analysis provides nuanced insights into the interplay between microbial community dynamics and seawater biogeochemistry. The first and third Principal Components (PC1 and PC3, which were the components that explained the largest variance of the amines) account for 54.6 % and 8.0 % of the total variance, respectively. In summary, in PCA (b), pTMA and dDMA were aligned with nanophytoplankton (2–20 μm) which included cryptophytes (*Cryptomonas* spp.) and not with the biomass of larger phytoplankton (Fig. 4b).

Varimax rotation was applied to the factors extracted via Principal Axis Factoring to enhance interpretability by maximizing the variance of Factor loadings, resulting in more distinct and interpretable patterns (Jolliffe, 2002) using the same variables as those applied in the PCAs. All key parameters, detailed in Table 1, were included in the analyses to support a robust interpretation of the Principal Components. Five Factors were selected from the scree analysis, in sum explaining 69 % (Table 1a) and 71 % (Table 1b) of the total data variance, respectively. Table 1 presents the loadings of the variables on the five rotated Factors, indicating the strength of correlation of each variable and its respective factor. Loadings (positive or negative) above 0.2 (or below -0.2) were considered significant. Finally, Pearson correlations for all pairs of variables are presented in Fig. S6. Overall, the Factor Analysis reinforced the exploration of the combined contribution of alkylamines and other variables to the total variance observed in the previous PCA analyses. pTMA showed larger positive loadings in Factor 2 of Table 1(a) (along with nutrients and DMSP) and Factor 3 of Table 1(b) (with nanophytoplankton and *Cryptomonas* spp. and slightly with the V1 virus population). This suggests that pTMA mostly occurred in the nanophytoplankton size fraction (<20 μm), that typically harbours most of the DMSP (Stefels et al., 2007). Also in the pairwise correlation analysis (Fig. S6), pTMA was best positively correlated with phytoplankton cells between 2 and 7 μm , *Cryptomonas* spp. (Mantel statistical test r and p -value of 0.71 and

0.007, respectively), silicate (Mantel statistical test r and p -value of 0.63 and 0.01, respectively), as well as with DMSP (Mantel statistical test r and p -value of 0.51 and 0.034, respectively), PNF 10–20 μm (Mantel statistical test r and p -value of 0.37 and 0.037, respectively), HNF and particularly HNF 2–5 μm (Mantel statistical test r and p -value of 0.49 and 0.03, respectively). Conversely, it was negatively correlated with big diatoms ($>40\text{ }\mu\text{m}$) ($p<0.1$). Dissolved TMA showed its largest negative and positive loadings in Factor 1 and 3 of Table 1(a), together with chlorophyll-a and particulate organic matter, and Factor 1 and 4 of Table 1(b), where it was essentially correlated with nanophytoplankton. Indeed, in the correlation matrix (Fig. S6) dTMA correlated with phytoplankton cells between 7 and 15 μm (Mantel statistical test r and p -value of 0.53 and 0.025, respectively), and more generally with phytoplankton cells ranging from 2 to 20 μm (Mantel statistical test r and p -value of 0.45 and 0.004, respectively).

Dissolved DMA contributed significantly to Factor 2 in Table 1(a) and similarly in several Factors in Table 1(b), concurring with pTMA, DMSP, photosynthetic cells in the 2–20 μm size range, HNA Bacteria, and nutrients (particularly silicate). In the correlation matrix (Fig. S6), dDMA was positively correlated with particulate TMA (Mantel statistical test r and p -value of 0.60 and 0.029, respectively), *Cryptomonas* spp. (Mantel statistical test r and p -value of 0.65 and 0.043, respectively), DMSP (Mantel statistical test r and p -value of 0.61 and 0.017, respectively), silicate (Mantel statistical test r and p -value of 0.72 and 0.004, respectively), nanoflagellate abundances, PNF (10–20 μm), HNF, and small HNF (2–5 μm) (Mantel statistical test r and p -value of 0.52 and 0.02, respectively).

Dissolved DEA had several similar positive and negative loadings in Table 1(a), which was also contributed by bacteria and general phytoplankton biomasses, and F_v'/F_m' . Additionally, dDEA contributed principally to Factor 5 in Table 1(b) together with HNA Bacteria. In pairwise correlations (Fig. S6), dDEA showed positive correlations with F_v'/F_m' (also indicated by the Mantel statistical test with r and p -value, 0.24 and, 0.038, respectively) and DMS (Mantel statistical test with r and p -value, 0.45, 0.046, respectively), and with dinoflagellate cysts, small dinoflagellates (10–20 μm) and big diatoms ($>40\text{ }\mu\text{m}$) ($p<0.1$).

Finally, dMMA, which was excluded from the PCA and Factor analysis as it was below detection limit in most cases, is known to originate primarily from the bacterial degradation of N-containing osmolytes and amino acids (Lidbury et al., 2015b; Mausz and Chen, 2019). dMMA exhibited a

619 significant positive correlation with DOC (Mantel statistical test r and p-value of 0.49 and 0.016,
620 respectively) and TOC (Mantel statistical test r and p-value of 0.48 and 0.02, respectively,) and
621 negative correlation with total and HNA bacteria biomass (Mantel statistical test r and p-value of
622 -0.28 and 0.04, respectively), salinity (Mantel statistical test r and p-value of -0.43 and 0.012,
623 respectively), and SST (Fig. S6).

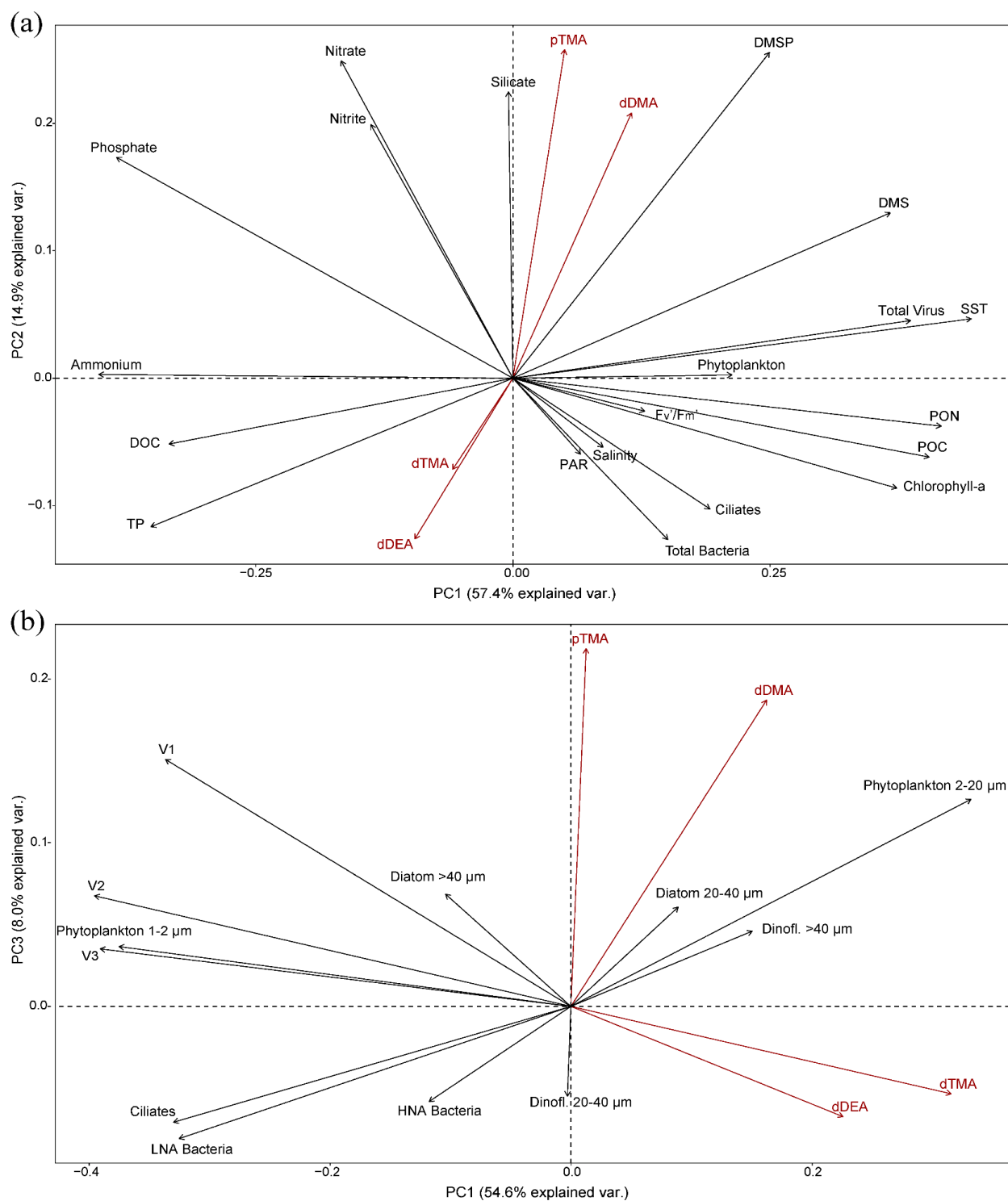


Figure 4. Principal component analyses of the highest explanatory biogeochemical parameters in the 18 underway seawater samples collected (see text). (a) PC2 vs PC1 of all physical and biogeochemical data from the water samples and the biomass of the main phytoplankton groups and viral, bacterial and ciliate biomasses and (b) PC3 vs PC1 of the more specific PCA run considering the biomasses of size-resolved phytoplankton types and ciliates, active and non-active bacterial cells and the virus fractions. The percentage of explained variance is given on each principal component axis. Amine forms are in red to facilitate visualization.

Table 1. Factor Analysis loadings corresponding to the PCA analyses shown in Fig. 4, after Varimax rotation. The upper part of the Table, Variables (a) refers to PCA (a) (Fig. 4a), while the bottom part refers to PCA (b) (Fig. 4b). Loadings above 0.2 (or below -0.2) (significant loadings) are shown in italics, and above 0.6 (or below -0.6) in bold italics. The last two lines of each table refer to the total variance explained by one factor in the data (SS Loadings) and to the proportion of the total variance in the dataset (Proportion Var.).

Variables (a)	Factor 1	Factor 2	Factor 3	Factor 4	Factor 5
pTMA	0.1	<i>0.50</i>	<i>-0.21</i>	0.03	<i>0.30</i>
dTMA	<i>-0.40</i>	-0.08	<i>0.41</i>	-0.14	0.00
dDMA	0.11	<i>0.74</i>	<i>0.44</i>	-0.07	0.09
dDEA	<i>-0.25</i>	0.01	<i>0.39</i>	<i>0.32</i>	<i>-0.35</i>
Chlorophyll-a	<i>0.26</i>	-0.10	<i>0.85</i>	0.10	<i>0.31</i>
SST	<i>0.92</i>	0.15	<i>0.24</i>	0.12	<i>0.29</i>
Salinity	0.03	0.09	<i>0.20</i>	<i>0.96</i>	-0.05
F _v '/F _m '	0.06	0.00	0.03	<i>0.72</i>	0.18
PAR	-0.07	0.13	<i>0.51</i>	<i>0.26</i>	-0.10
DMSP	0.10	<i>0.58</i>	<i>0.25</i>	-0.04	<i>0.68</i>
DMS	<i>0.43</i>	0.16	0.09	0.05	<i>0.70</i>
Total Bacteria	<i>0.47</i>	-0.10	0.12	<i>0.41</i>	<i>-0.28</i>
Total Virus	<i>0.87</i>	0.09	0.05	0.09	<i>0.25</i>
Phytoplankton	-0.17	-0.16	0.19	<i>0.27</i>	<i>0.74</i>
Ciliates	<i>0.55</i>	-0.28	-0.12	-0.05	0.02
Nitrate	-0.13	<i>0.69</i>	<i>-0.35</i>	0.16	0.01
Nitrite	-0.03	<i>0.57</i>	-0.11	<i>-0.24</i>	-0.09
Ammonium	<i>-0.80</i>	0.04	-0.25	0.05	-0.15
Silicate	-0.06	<i>0.91</i>	<i>0.29</i>	<i>0.25</i>	0.00
Phosphate	<i>-0.51</i>	<i>0.55</i>	<i>-0.45</i>	0.09	<i>-0.22</i>
DOC	<i>-0.40</i>	0.01	0.02	<i>-0.48</i>	<i>-0.52</i>
PON	<i>0.39</i>	-0.01	<i>0.74</i>	0.09	<i>0.42</i>
POC	<i>0.35</i>	-0.07	<i>0.74</i>	0.13	<i>0.41</i>
TP	<i>-0.27</i>	-0.03	-0.17	0.13	<i>-0.72</i>
SS Loadings	4.10	3.28	3.37	2.34	3.30
Proportion Var.	0.17	0.14	0.14	0.10	0.14

Variables (b)	Factor 1	Factor 2	Factor 3	Factor 4	Factor 5
pTMA	0.00	-0.14	0.93	0.02	-0.02
dTMA	-0.30	0.21	-0.18	-0.46	-0.03
dDMA	0.08	0.09	0.41	-0.54	0.40
dDEA	-0.19	0.06	-0.24	-0.4	0.47
HNA Bacteria	0.15	0.46	-0.15	0.44	0.61
LNA Bacteria	0.29	0.07	-0.05	0.76	0.15
V1	0.85	0.37	0.30	0.15	0.04
V2	0.87	0.01	0.10	0.17	-0.06
V3	0.81	0.10	0.04	0.26	0.02
Phytoplankton 1–2 µm	0.95	-0.04	-0.11	-0.04	-0.03
Phytoplankton 2–20 µm	-0.31	0.45	0.36	-0.42	-0.05
Diatoms 20–40 µm	0.10	0.94	-0.09	-0.14	0.09
Diatoms >40 µm	0.18	0.82	0.03	0.37	0.09
Dinofl. 20–40 µm	0.04	0.04	-0.07	-0.05	-0.55
Dinofl. >40 µm	0.00	0.93	-0.09	-0.22	-0.05
Ciliates	0.62	0.00	-0.20	0.19	-0.05
SS Loadings	3.84	3.04	1.51	1.97	1.15
Proportion Var.	0.24	0.19	0.09	0.12	0.07

4 Discussion

4.1 Alkylamine distributions

The almost exclusive detection of TMA in particles suggests that this may be the predominant form of methylated amines within cells. Release from cells explains that dissolved TMA is consistently present in all our seawater samples, together with the fact that TMA has the lowest Henry's constant, indicating it is the most soluble amine. This tertiary amine is known to be the primary compound released during the decomposition of marine algae and microorganisms, marsh grasses and fish, mainly as a breakdown product of quaternary amine precursors (Mausz and Chen, 2019; Sun et al., 2019). Three other alkylamines were detected dissolved in seawater. Their distributions varied across regions around the Antarctic Peninsula: the samples off the Western Antarctic Peninsula harboured different total dissolved amine concentrations (78.3 ± 44.7 nM; $n=7$) from those from the northern Weddell Sea (42.4 ± 24.9 nM; $n=12$) (Fig. 2a). This coincided

with higher Chl-a levels west of the Antarctic Peninsula (Fig. 1, Table S2 and Fig. S5). Also, F_v'/F_m' values were slightly higher in samples from the Antarctic Peninsula, indicating greater photosynthetic efficiency and suggesting that in this area phytoplankton were in better physiological condition than in the Weddell Sea. Given the similarities in phytoplankton abundances and composition of the two areas, this difference can likely be attributed to the potential effect of light stress, since waters of the Weddell Sea were clearer and more stratified (data not shown), hence more exposed to excess of damaging sunlight. Most samples were collected at 18:00 local time, which corresponds to daylight hours during the Austral summer. Potential diel variations in amine concentrations should be taken into account in future studies.

Amines have been measured in seawater in polar regions primarily by Gibb and Hatton (2004), who used a flow-diffusion gas chromatography method with selective nitrogen detection in Marguerite Bay, Antarctica, and by Dall'Osto et al. (2017, 2019), with subsequent methodological improvements introduced by Akenga and Fitzsimons (2024). Gibb and Hatton (2004) reported maximum dMMA concentrations of 36 nM, while Dall'Osto et al. (2017, 2019) observed concentrations of total methylated amines (3–10 nM) that were significantly lower than those measured in the present study. Here, we found regional differences in the composition of the alkylamine mixture. In the proximity to the Western Antarctic Peninsula, dMMA was absent, with dDMA dominating, contributing up to 64 % of the total dissolved amines, followed by dTMA with a 27 % contribution and dDEA with 9 % (Fig. 2a). Conversely, samples collected within the Weddell Sea exhibited a distinct composition, with TMA comprising the highest proportion at 50 %, followed by dDMA at 27 %, dDEA at 16 % and dMMA at 7 %. In this study, dDEA concentrations are similar to the range reported by van Pinxteren et al. (2019) for the SML and seawater in tropical waters (9 to 23 nM). Overall, alkylamines can be released through various processes, including excretion by primary producers and bacterial activity, protist egestion, sloppy feeding by predators, and viral lysis (Bronk, 2002). This agrees with the fact that phytoplankton and bacteria function as DON producers (Antia et al., 1991; Bronk, 2002; Wheeler et al., 1974; Wheeler and Kirchman, 1986).

Phytoplankton release DON actively through mechanisms such as osmotic adjustments, reduced N excretion in response to changes in light, and autolysis. Phytoplanktonic passive release can occur due to physiological stress induced by factors such as ultraviolet radiation, temperature

fluctuations, and light variations, as well as interactions with microzooplankton grazing and viral infections leading to lysis (Bronk, 2002). Viruses further contribute to DON production by inducing host cell lysis during the final stages of infection, releasing the cellular contents into the environment (Bronk, 2002). Similar processes are expected to occur with methylated amines (Sun et al., 2019). Releasing N-rich dissolved organic matter (DOM) demands considerable energy from healthy phytoplankton cells (Ward and Bronk, 2001). In the Southern Ocean, N is generally not limiting because its use is limited by Fe and light; however, in the Western Antarctic Peninsula, where primary production can likely be supplied with Fe and other micronutrients from land, inorganic N may become depleted in phytoplankton blooms reaching limiting levels, as observed in Dittrich et al. (2022). Under these specific conditions, phytoplankton can also act as DON consumers, and the recycling of phytoplankton-released DON may provide an essential, bioavailable N source for sustaining phytoplankton growth. Notably, it has been reported that phytoplankton like the chlorophyte *Platymonas* (phototrophic nanoflagellate) incorporate primary amines from natural seawater efficiently, potentially supporting robust growth (North, 1975). Similarly, diatoms have demonstrated efficient uptake of alkylamines (Wheeler and Hellebust, 1981).

Bacteria are identified as the primary consumers and transformers of organic matter, as evidenced by the relationships between bacterial abundance and DON and DOC concentrations (Fig. S6). Furthermore, methylamine-degrading bacteria play a crucial role in releasing bioavailable N from alkylamines, which supports diatom growth, while diatoms provide organic C to bacteria in a mutualistic exchange (Stein, 2017; Suleiman et al., 2016). Moreover, marine bacteria metabolize methylamines as a N source via different pathways facilitating direct assimilation of N into biomass (Lidbury et al., 2015b; Sun et al., 2019; Taubert et al., 2017). This recycling of amines may explain their nanomolar concentrations in seawater, suggesting they may serve as valuable organic N sources for both phytoplankton and bacteria. Given their volatile nature, alkylamines are also expected to be lost to the atmosphere. The cycle of methylated amines shares several similarities with the cycles of methylated sulfur compounds, such as DMSP and DMS, in the marine environment. Both methylated amines and sulfur compounds originate from marine phytoplankton and participate in atmospheric processes. Recent studies have shown that TMA monooxygenase, an enzyme in marine bacteria, can oxidise both TMA and dimethylsulfide (Chen

et al., 2011; Lidbury et al., 2016). Thus, parallelisms between marine methylated amines and DMS metabolism underscores the importance of studying these molecules in tandem.

4.2 Correlations between alkylamines, chemical and environmental variables, and the microbial community

Using PCA, Factor Analysis, pairwise correlation analyses and statistical Mantel test, we found that TMA appears to be predominantly produced intracellularly by nanophytoplankton. Subsequently, it is released into the environment through cellular stress, mortality, or even by mechanical processes like filtration during sampling. This could explain the observed pairwise opposite correlation between particulate and dissolved TMA. The production of TMA is likely linked to the enzymatic activity of TMAO reductase (Mausz and Chen, 2019), an enzyme which, like dimethyl sulfoxide reductase (Spiese et al., 2009), occurs in marine bacteria but is potentially common in phytoplankton cells too. This enzyme reduces TMAO, a prevalent osmolyte like glycine betaine in phytoplankton (Gibb and Hatton, 2004). Dissolved DMA appears to exhibit a causal relationship with particulate TMA, suggesting a shared phenomenology or a common origin. The statistical associations suggest that dDMA is linked to nanophytoplankton, potentially originating from the degradation of TMA or TMAO by bacteria or phytoplankton themselves. In aerobic conditions, DMA is produced from TMAO via TMAO demethylase (Barrett and Kwan, 1985; Lidbury et al., 2014). Although TMAO demethylase activity has not yet been reported in phytoplankton, its presence in fish tissues (Kimura et al., 2000) and the direct evidence of TMAO occurrence in polar diatoms (Dawson et al., 2020; Fitzsimons et al., 2024) suggest that this enzyme may also occur in eukaryotic microalgae. Although the involvement of a TMAO demethylation or any other enzyme requires genomic confirmation, our findings suggest that phytoplankton could directly release DMA or indirectly through bacteria attached to the outer membrane or residing in the phycosphere. In tropical waters, van Pinxteren et al. (2019) reported positive correlation between amines and pigments (fucoxanthin and chlorophyll-a) suggesting that amine production was fuelled by algal metabolism, most likely diatoms. In our study in polar waters, we found that TMA and dissolved DMA were closely related to nanosized phytoplankton.

Overall, dDEA exhibited an inverse correlation with particulate TMA. Notably, dDEA did not display a strong distributional alignment with any specific microbial variables, although a weak association with active bacteria was observed. Additionally, dDEA showed a moderate positive

correlation with the photosynthetic efficiency of phytoplankton cells (F_v'/F_m') and with different phytoplankton groups compared to MAs. As expected, F_v'/F_m' displayed an inverse relationship to nutrient availability. In the Southern Ocean, F_v'/F_m' declines when iron availability limits primary productivity despite the presence of elevated macronutrient concentrations (Wu et al., 2019). Although the precise source of dDEA remains unclear, these findings demonstrate that DEA is widespread in Antarctic waters and follows distinct biological and biogeochemical pathways compared to MAs. We speculate that DEA may be formed by degradation of an amino acid precursor, potentially proline, considered an important N-bearing osmolyte (Fitzsimons et al., 2024). However, further research is needed to identify its specific origins and the processes governing its distribution. Finally, regarding dMMA, the labile and volatile nature of this compound suggest that bacteria efficiently remineralize dMMA into ammonium (Lidbury et al., 2015b), and that MMA volatilizes quickly to the atmosphere, both processes contributing to the rapid depletion of MMA in surface waters. Zhang et al. (2023) demonstrated that elevated salinity enhances the tendency of amines to volatilize from surface seawater by suppressing amine ionisation, thereby increasing exchange fluxes.

Altogether, the multivariate and pairwise correlation analyses make us concur with previous works in that phytoplankton are the primary producers of amines or amine precursors (Fitzsimons et al., 2023; van Pinxteren et al., 2019; Poste et al., 2014). However, we identify nanophytoplankton and *Cryptomonas* spp. populations, instead of diatoms, as the main responsible for TMA and DMA production in Antarctic waters in late summer. Smaller phytoplankton, likely those that are better adapted to thrive under iron-limited conditions (Schoffman et al., 2016), would synthesise and harbour most of the intracellular TMA. Part of it would be released likely through processes such as cell mortality or through physiologically-driven DOM excretion. Likewise, DMA was statistically associated with small phytoplankton cells and heterotrophic nanoflagellates (PNF and HNF, respectively) as well as DMSP, exhibiting a distribution similar to the sulfur osmolyte. DMA was more closely associated with phytoplankton than with bacteria, which are expected to be responsible for TMA demethylation into DMA. This suggests that DMA is largely produced from phytoplankton TMA or TMAO by the algal cells themselves or closely associated bacteria. Finally, the distribution of DEA suggests distinct biogeochemical pathways compared to methylamines, potentially involving larger phytoplankton and bacterial communities. Notably, the factor most strongly linked to mortality, viruses, did not appear to influence alkylamine pathways. However,

incorporating viral lysis as a key phenomenon in Antarctic phytoplankton dynamics is essential for advancing the understanding of microbial interactions and improving the accuracy of organic matter flux estimations in this climate-sensitive region (Biggs et al., 2021).

Our findings indicate that alkylamine distributions are linked to microplankton trophic webs, in particular to certain phytoplankton cell size groups and ecophysiological conditions rather than to total biomass. Our approach does not allow us to quantify how much of the amines are produced directly by phytoplankton or through bacterial reworking of phytoplankton metabolites, yet we provide indications that both processes occur. Dissolved and particulate alkylamines accounted for non-negligible proportions of DON (ca. 1.8 %, with a maximum of 8.7 %), and of PON (ca. 1.5 %, with a maximum of 3.1 %). These proportions are reported here for the first time, providing a novel insight into the quantitative contribution of alkylamines to marine organic N pools.

This study contributes to the necessity of increasing alkylamine determinations to be incorporated into future biogeochemical and climate models, given the pivotal role of alkylamines in both marine and atmospheric systems. In the Southern Ocean, biogenic emissions influence aerosol numbers through primary and secondary pathways, potentially enhancing CCN concentrations and modulating cloud albedo, thereby impacting regional radiative forcing (McCoy et al., 2015). Low-molecular-weight alkylamines contribute to both new particle formation (Brean et al., 2021) and aerosol growth, particularly in air masses passing over melting sea ice (Dall'Osto et al., 2017). Incorporating alkylamines in climate models for this climate-sensitive region requires gaining understanding of their distribution and drivers. The present study represents a step forward towards this aim.

5 Conclusion

Alkylamines are seawater compounds whose role as precious organic nutrients in N transfer among trophic levels is starting to emerge. Despite their increasingly recognized importance, the distribution, biological sources, formation mechanisms, and emission strength of marine amines remain poorly known. This study provides several significant advances in the knowledge of the drivers of marine alkylamine concentrations and speciation. Overall, our results emphasise that alkylamines are embedded within marine microbial food webs, where phytoplankton, bacteria and viruses are interconnected, thereby influencing nutrient cycling, microbial dynamics, and the overall health of marine ecosystems. Our study, conducted under varying biogeochemical

conditions, reveals that tri- and dimethylamine present in Antarctic surface waters were primarily sourced from nanophytoplankton cells and the associated bacteria and heterotrophic nanoflagellates, and diethylamine from hitherto unknown processes. Describing the distribution and behavior of alkylamines in the surface ocean is pivotal for understanding their roles in marine biogeochemical cycles, atmospheric chemistry, and climate.

6 Author Contributions

AR, MD'O, RS, and EB conceptualized and designed the study. AR and AS collected seawater and amine samples during the PolarChange Expedition. AR, under the supervision of MFF and PA, processed and analyzed the amine samples, generating the amine dataset. MFF provided essential resources for the amine analysis. ELS, QG, MV, DV, CW, RS, and EB participated in the expedition, collected samples, and conducted biogeochemical and biological analyses. YMC and AR processed and analyzed flow cytometry samples at ICM. AR performed the statistical analyses, prepared the figures, and drafted the manuscript's first version. AR, MFF, PA, CW, RS, and EB contributed to data interpretation and manuscript writing. All authors reviewed, revised, and approved the final version of the manuscript.

7 Data availability

All data are provided in the Supplementary Information file.

8 Competing Interests

The authors declare that they have no conflict of interest.

9 Acknowledgements

We would like to thank the crew of the RV *Hesperides* for the logistic support, making possible the data collection of this study. Special thanks to Mara Abad and Núria González Fernández for TOC, TN and nutrient analyses at the Chemistry Service of the ICM-CSIC. We thank Jair Antonio Arévalo Lirio and Sofía Ibáñez Homedes for assistance counting flagellates and bacteria.

10 Financial support

AR was supported by the FPI grant (PRE2020-092994) from the Spanish Ministerio de Ciencia e Innovación (MICIN) and European Social Fund (ESF) ‘Investing in your Future’. The POLARCHANGE project (PID2019-110288RB-I00) also received funding from the Spanish Ministerio de Ciencia e Innovación (MICIN). Further support was provided through an Advanced Grant from the European Research Council (ERC-2018-AdG #834162). This study is part of the POLARCSIC platform activities, and had the institutional support of the ‘Severo Ochoa Centre of Excellence’ accreditation (CEX2019-000928-S) to the ICM-CSIC.

11 References

- Akenga, P. C. and Fitzsimons, M. F.: Automated method for the sensitive analysis of volatile amines in seawater, *ACS ES T Water*, 4, 2504–2510, <https://doi.org/10.1021/acsestwater.4c00007>, 2024.
- Álvarez-Salgado, X. A. and Miller, A. E. J.: Simultaneous determination of dissolved organic carbon and total dissolved nitrogen in seawater by high temperature catalytic oxidation: conditions for precise shipboard measurements, *Mar. Chem.*, 62, 325–333, [https://doi.org/10.1016/s0304-4203\(98\)00037-1](https://doi.org/10.1016/s0304-4203(98)00037-1), 1998.
- Antia, N. J., Harrison, P. J., and Oliveira, L.: The role of dissolved organic nitrogen in phytoplankton nutrition, cell biology and ecology, *Phycologia*, 30, 1–89, <https://doi.org/10.2216/i0031-8884-30-1-1.1>, 1991.
- Auguie, B.: gridExtra: Miscellaneous Functions for "Grid" Graphics, Comprehensive R Archive Network (CRAN), 2017.
- Barrett, E. L. and Kwan, H. S.: Bacterial reduction of trimethylamine oxide, *Annu. Rev. Microbiol.*, 39, 131–149, <https://doi.org/10.1146/annurev.mi.39.100185.001023>, 1985.
- Biggs, T. E. G., Huisman, J., and Brussaard, C. P. D.: Viral lysis modifies seasonal phytoplankton dynamics and carbon flow in the Southern Ocean, *ISME J.*, 15, 3615–3622, <https://doi.org/10.1038/s41396-021-01033-6>, 2021.
- Bolar, K.: STAT: Interactive Document for Working with Basic Statistical Analysis, Comprehensive R Archive Network (CRAN), 2019.
- Brean, J., Dall’Osto, M., Simó, R., Shi, Z., Beddows, D. C. S., and Harrison, R. M.: Open ocean and coastal new particle formation from sulfuric acid and amines around the Antarctic Peninsula, *Nat. Geosci.*, 14, 383–388, <https://doi.org/10.1038/s41561-021-00751-y>, 2021.

861 Bronk, D. A.: Dynamics of DON, in: Biogeochemistry of Marine Dissolved Organic Matter,
 862 Elsevier, 153–247, <https://doi.org/10.1016/b978-012323841-2/50007-5>, 2002.

863 Brussaard, C. P. D.: Optimization of procedures for counting viruses by flow cytometry, Appl.
 864 Environ. Microbiol., 70, 1506–1513, <https://doi.org/10.1128/AEM.70.3.1506-1513.2004>, 2004.

865 Brussaard, C. P. D., Thyrrhaug, R., Marie, D., and Bratbak, G.: Flow cytometric analyses of viral
 866 infection in two marine phytoplankton species, *Micromonas pusilla* (prasinophyceae) and
 867 *Phaeocystis pouchetii* (prymnesiophyceae), J. Phycol., 35, 941–948,
 868 <https://doi.org/10.1046/j.1529-8817.1999.3550941.x>, 1999.

869 Brussaard, C. P. D., Mari, X., Van Bleijswijk, J. D. L., and Veldhuis, M. J. W.: A mesocosm study
 870 of *Phaeocystis globosa* (Prymnesiophyceae) population dynamics, Harmful Algae, 4, 875–893,
 871 <https://doi.org/10.1016/j.hal.2004.12.012>, 2005.

872 Burg, M. B. and Ferraris, J. D.: Intracellular organic osmolytes: function and regulation, J. Biol.
 873 Chem., 283, 7309–7313, <https://doi.org/10.1074/jbc.R700042200>, 2008.

874 Chen, Y., Patel, N. A., Crombie, A., Scrivens, J. H., and Murrell, J. C.: Bacterial flavin-containing
 875 monooxygenase is trimethylamine monooxygenase, Proc. Natl. Acad. Sci. U. S. A., 108, 17791–
 876 17796, <https://doi.org/10.1073/pnas.1112928108>, 2011.

877 Chistoserdova, L., Kalyuzhnaya, M. G., and Lidstrom, M. E.: The expanding world of
 878 methylotrophic metabolism, Annu. Rev. Microbiol., 63, 477–499,
 879 <https://doi.org/10.1146/annurev.micro.091208.073600>, 2009.

880 Corral, A. F., Choi, Y., Collister, B. L., Crosbie, E., Dadashazar, H., Digangi, J. P., Diskin, G.,
 881 Fenn, M. A., Kirschler, S., Moore, R., Nowak, J. B., Shook, M., Stahl, C., Shingler, T. J., Thornhill,
 882 K., Voigt, C., Ziemba, L., and Sorooshian, A.: Alkyl amines in cloud water: A case study over the
 883 northwest Atlantic ocean, Environ. Sci. Atmos., <https://doi.org/10.1039/d2ea00117a>, 2022.

884 Cree, C. H. L., Airs, R., Archer, S. D., and Fitzsimons, M. F.: Measurement of methylamines in
 885 seawater using solid phase microextraction and gas chromatography, Limnol. Oceanogr. Methods,
 886 16, 411–420, <https://doi.org/10.1002/lom3.10255>, 2018.

887 Dall'Osto, M., Ovadnevaite, J., Paglione, M., Beddows, D. C. S., Ceburnis, D., Cree, C., Cortés,
 888 P., Zamanillo, M., Nunes, S. O., Pérez, G. L., Ortega-Retuerta, E., Emelianov, M., Vaqué, D.,
 889 Marrasé, C., Estrada, M., Sala, M. M., Vidal, M., Fitzsimons, M. F., Beale, R., Airs, R., Rinaldi,
 890 M., Decesari, S., Cristina Facchini, M., Harrison, R. M., O'Dowd, C., and Simó, R.: Antarctic sea
 891 ice region as a source of biogenic organic nitrogen in aerosols, Sci. Rep., 7, 6047,
 892 <https://doi.org/10.1038/s41598-017-06188-x>, 2017.

893 Dall'Osto, M., Airs, R. L., Beale, R., Cree, C., Fitzsimons, M. F., Beddows, D., Harrison, R. M.,
 894 Ceburnis, D., O'Dowd, C., Rinaldi, M., Paglione, M., Nenes, A., Decesari, S., and Simó, R.:
 895 Simultaneous Detection of Alkylamines in the Surface Ocean and Atmosphere of the Antarctic
 896 Sympagic Environment, ACS Earth Space Chem., 3, 854–862,
 897 <https://doi.org/10.1021/acsearthspacechem.9b00028>, 2019.

898 Dawson, H. M., Heal, K. R., Torstensson, A., Carlson, L. T., Ingalls, A. E., and Young, J. N.:
 899 Large diversity in nitrogen- and sulfur-containing compatible solute profiles in polar and temperate
 900 diatoms, *Integr. Comp. Biol.*, 60, 1401–1413, <https://doi.org/10.1093/icb/icaa133>, 2020.

901 Dittrich, R., Henley, S. F., Ducklow, H. W., and Meredith, M. P.: Dissolved organic carbon and
 902 nitrogen cycling along the west Antarctic Peninsula during summer, *Prog. Oceanogr.*, 206,
 903 102854, <https://doi.org/10.1016/j.pocean.2022.102854>, 2022.

904 Edler, L. and Elbrächter, M.: The Utermöhl method for quantitative phytoplankton analysis.
 905 Microscopic and molecular methods for quantitative phytoplankton analysis, 2010.

906 Evans, C., Pearce, I., and Brussaard, C. P. D.: Viral-mediated lysis of microbes and carbon release
 907 in the sub-Antarctic and Polar Frontal zones of the Australian Southern Ocean, *Environ.*
 908 *Microbiol.*, 11, 2924–2934, <https://doi.org/10.1111/j.1462-2920.2009.02050.x>, 2009.

909 Facchini, M. C., Decesari, S., Rinaldi, M., Carbone, C., Finessi, E., Mircea, M., Fuzzi, S., and
 910 O'Dowd, C. D.: Important source of marine secondary organic aerosol from biogenic amines,
 911 *Environ. Sci. Technol.*, 42(24), 9116–9121, <https://doi.org/10.1021/es8018385>, 2008.

912 Fitzsimons, M. F., Tilley, M., and Cree, C. H. L.: The determination of volatile amines in aquatic
 913 marine systems: A review, *Anal. Chim. Acta*, 1241, 340707,
 914 <https://doi.org/10.1016/j.aca.2022.340707>, 2023.

915 Fitzsimons, M. F., Airs, R., and Chen, Y.: The occurrence and biogeochemical cycling of
 916 quaternary, ternary and volatile amines in marine systems, *Front. Mar. Sci.*, 11,
 917 <https://doi.org/10.3389/fmars.2024.1466221>, 2024.

918 Gasol, J. M. and Del Giorgio, P. A.: Using flow cytometry for counting natural planktonic bacteria
 919 and understanding the structure of planktonic bacterial communities, *Sci. Mar.*, 64, 197–224,
 920 <https://doi.org/10.3989/scimar.2000.64n2197>, 2000.

921 Gibb, S. W. and Hatton, A. D.: The occurrence and distribution of trimethylamine-N-oxide in
 922 Antarctic coastal waters, *Mar. Chem.*, 91, 65–75, <https://doi.org/10.1016/j.marchem.2004.04.005>,
 923 2004.

924 Gibb, S. W., Mantoura, R. F. C., and Liss, P. S.: Ocean-atmosphere exchange and atmospheric
 925 speciation of ammonia and methylamines in the region of the NW Arabian Sea, *Global*
 926 *Biogeochem. Cycles*, 13, 161–178, <https://doi.org/10.1029/98gb00743>, 1999.

927 Goldwhite, H.: Nitrogen derivatives of the aliphatic hydrocarbons, in: *Rodd's Chemistry of Carbon*
 928 *Compounds*, Elsevier, 93–164, <https://doi.org/10.1016/b978-044453345-6.50475-2>, 1964.

929 Gorbunov, M. Y. and Falkowski, P. G.: Using chlorophyll fluorescence to determine the fate of
 930 photons absorbed by phytoplankton in the world's oceans, *Ann. Rev. Mar. Sci.*, 14, 213–238,
 931 <https://doi.org/10.1146/annurev-marine-032621-122346>, 2022.

932 Gorbunov, M. Y., Shirsin, E., Nikonova, E., Fadeev, V. V., and Falkowski, P. G.: A multi-spectral
 933 fluorescence induction and relaxation (FIRE) technique for physiological and taxonomic analysis

934 of phytoplankton communities, *Mar. Ecol. Prog. Ser.*, 644, 1–13,
 935 <https://doi.org/10.3354/meps13358>, 2020.

936 Grasshoff, K., Ehrhardt, M., and Kremling, K.: *Methods of Seawater Analysis*, 1983.

937 Jakobsen, H. H. and Markager, S.: Carbon-to-chlorophyll ratio for phytoplankton in temperate
 938 coastal waters: Seasonal patterns and relationship to nutrients, *Limnol. Oceanogr.*, 61, 1853–1868,
 939 <https://doi.org/10.1002/lno.10338>, 2016.

940 Jolliffe, I. T.: Principal component analysis for special types of data, in: *Principal Component*
 941 *Analysis*, Springer, New York, NY, 338–372, https://doi.org/10.1007/0-387-22440-8_13, 2002.

942 Kassambara, A.: ggcorrplot: Visualization of a Correlation Matrix Using “ggplot2”,
 943 Comprehensive R Archive Network (CRAN), 2021.

944 Kassambara, A. and Mundt, F.: factoextra: Extract and Visualize the Results of Multivariate Data
 945 Analyses, Comprehensive R Archive Network (CRAN), 2020.

946 Kimura, M., Seki, N., and Kimura, I.: Occurrence and some properties of trimethylamine-N-oxide
 947 demethylase in myofibrillar fraction from walleye pollack muscle, *Fish. Sci.*, 66, 725–729,
 948 <https://doi.org/10.1046/j.1444-2906.2000.00118.x>, 2000.

949 Kinsey, J. D. and Kieber, D. J.: Microwave preservation method for DMSP, DMSO, and acrylate
 950 in unfiltered seawater and phytoplankton culture samples: Microwave Sample Preservation
 951 Method, *Limnol. Oceanogr. Methods*, 14, 196–209, <https://doi.org/10.1002/lom3.10081>, 2016.

952 Koester, I., Quinlan, Z. A., Nothias, L.-F., White, M. E., Rabines, A., Petras, D., Brunson, J. K.,
 953 Dührkop, K., Ludwig, M., Böcker, S., Azam, F., Allen, A. E., Dorrestein, P. C., and Aluwihare,
 954 L. I.: Illuminating the dark metabolome of Pseudo-nitzschia-microbiome associations, *Environ.*
 955 *Microbiol.*, 24, 5408–5424, <https://doi.org/10.1111/1462-2920.16242>, 2022.

956 Landa, M., Burns, A. S., Roth, S. J., and Moran, M. A.: Bacterial transcriptome remodeling during
 957 sequential co-culture with a marine dinoflagellate and diatom, *ISME J.*, 11, 2677–2690,
 958 <https://doi.org/10.1038/ismej.2017.117>, 2017.

959 Lidbury, I., Murrell, J. C., and Chen, Y.: Trimethylamine N-oxide metabolism by abundant marine
 960 heterotrophic bacteria, *Proc. Natl. Acad. Sci. U. S. A.*, 111, 2710–2715,
 961 <https://doi.org/10.1073/pnas.1317834111>, 2014.

962 Lidbury, I., Kimberley, G., Scanlan, D. J., Murrell, J. C., and Chen, Y.: Comparative genomics
 963 and mutagenesis analyses of choline metabolism in the marine *Roseobacter* clade, *Environ.*
 964 *Microbiol.*, 17, 5048–5062, <https://doi.org/10.1111/1462-2920.12943>, 2015a.

965 Lidbury, I., Kröber, E., Zhang, Z., Zhu, Y., Murrell, J. C., Chen, Y., and Schäfer, H.: A mechanism
 966 for bacterial transformation of dimethylsulfide to dimethylsulfoxide: a missing link in the marine
 967 organic sulfur cycle, *Environ. Microbiol.*, 18, 2754–2766, [https://doi.org/10.1111/1462-](https://doi.org/10.1111/1462-2920.13354)
 968 [2920.13354](https://doi.org/10.1111/1462-2920.13354), 2016.

969 Lidbury, I. D. E. A., Murrell, J. C., and Chen, Y.: Trimethylamine and trimethylamine N-oxide
 970 are supplementary energy sources for a marine heterotrophic bacterium: implications for marine
 971 carbon and nitrogen cycling, *ISME J.*, 9, 760–769, <https://doi.org/10.1038/ismej.2014.149>, 2015b.

972 Liu, C., Li, H., Zheng, H., Wang, G., Qin, X., Chen, J., Zhou, S., Lu, D., Liang, G., Song, X.,
 973 Duan, Y., Liu, J., Huang, K., and Deng, C.: Ocean emission pathway and secondary formation
 974 mechanism of aminiums over the Chinese marginal sea, *J. Geophys. Res.*, 127,
 975 <https://doi.org/10.1029/2022jd037805>, 2022.

976 Marie, D., Rigaut-Jalabert, F., and Vaulot, D.: An improved protocol for flow cytometry analysis
 977 of phytoplankton cultures and natural samples: AnImproved Protocol for Flow Cytometry
 978 Analysis, *Cytometry A*, 85, 962–968, <https://doi.org/10.1002/cyto.a.22517>, 2014.

979 Masdeu-Navarro, M., Mangot, J.-F., Xue, L., Cabrera-Brufau, M., Gardner, S. G., Kieber, D. J.,
 980 González, J. M., and Simó, R.: Spatial and diel patterns of volatile organic compounds, DMSP-
 981 derived compounds, and planktonic microorganisms around a tropical scleractinian coral colony,
 982 *Front. Mar. Sci.*, 9, <https://doi.org/10.3389/fmars.2022.944141>, 2022.

983 Mausz, M. A. and Chen, Y.: Microbiology and ecology of methylated Amine metabolism in
 984 marine ecosystems, *Curr. Issues Mol. Biol.*, 33, 133–148, <https://doi.org/10.21775/cimb.033.133>,
 985 2019.

986 McCoy, D. T., Burrows, S. M., Wood, R., Grosvenor, D. P., Elliott, S. M., Ma, P.-L., Rasch, P. J.,
 987 and Hartmann, D. L.: Natural aerosols explain seasonal and spatial patterns of Southern Ocean
 988 cloud albedo, *Sci. Adv.*, 1, e1500157, <https://doi.org/10.1126/sciadv.1500157>, 2015.

989 Menden-Deuer, S. and Lessard, E. J.: Carbon to volume relationships for dinoflagellates, diatoms,
 990 and other protist plankton, *Limnol. Oceanogr.*, 45, 569–579,
 991 <https://doi.org/10.4319/lo.2000.45.3.0569>, 2000.

992 Ning, A., Liu, L., Zhang, S., Yu, F., Du, L., Ge, M., and Zhang, X.: The critical role of
 993 dimethylamine in the rapid formation of iodic acid particles in marine areas, *Npj Clim. Atmos.*
 994 *Sci.*, 5, <https://doi.org/10.1038/s41612-022-00316-9>, 2022.

995 Norland, S.: The relationship between biomass and volume of bacteria. In: *Handbook of Methods*
 996 *in Aquatic Microbial Ecology*, edited by P. Kemp, B. Sherr, E. Sherr, and J. Cole, Lewis
 997 Publishers, 1993.

998 North, B. B.: Primary amines in California coastal waters: Utilization by phytoplankton 1,
 999 *Limnology and Oceanography*, 20, 20–27, 1975.

1000 Oksanen, J.: vegan: Community Ecology Package, Comprehensive R Archive Network (CRAN),
 1001 2022.

1002 Palenik, B. and Morel, F. M.: Amine oxidases of marine phytoplankton, *Appl. Environ. Microbiol.*,
 1003 57, 2440–2443, <https://doi.org/10.1128/aem.57.8.2440-2443.1991>, 1991.

1004 van Pinxteren, M., Müller, C., Iinuma, Y., Stolle, C., and Herrmann, H.: Chemical characterization
 1005 of dissolved organic compounds from coastal sea surface microlayers (Baltic Sea, Germany),
 1006 *Environ. Sci. Technol.*, 46(19), 10455–10462, <https://doi.org/10.1021/es204492b>, 2012.

1007 van Pinxteren, M., Fomba, K. W., van Pinxteren, D., Triesch, N., Hoffmann, E. H., Cree, C. H. L.,
 1008 Fitzsimons, M. F., von Tümpling, W., and Herrmann, H.: Aliphatic amines at the Cape Verde
 1009 Atmospheric Observatory: Abundance, origins and sea-air fluxes, *Atmos. Environ.* (1994), 203,
 1010 183–195, <https://doi.org/10.1016/j.atmosenv.2019.02.011>, 2019.

1011 Poste, A. E., Grung, M., and Wright, R. F.: Amines and amine-related compounds in surface
 1012 waters: a review of sources, concentrations and aquatic toxicity, *Sci. Total Environ.*, 481, 274–
 1013 279, <https://doi.org/10.1016/j.scitotenv.2014.02.066>, 2014.

1014 Revelle, W.: psych: Procedures for Psychological, Psychometric, and Personality Research,
 1015 Comprehensive R Archive Network (CRAN), 2023.

1016 Rinaldi, M., Paglione, M., Decesari, S., Harrison, R. M., Beddows, D. C. S., Ovadnevaite, J.,
 1017 Ceburnis, D., O'Dowd, C. D., Simó, R., and Dall'Osto, M.: Contribution of Water-Soluble Organic
 1018 Matter from Multiple Marine Geographic Eco-Regions to Aerosols around Antarctica, *Environ.*
 1019 *Sci. Technol.*, 54, 7807–7817, <https://doi.org/10.1021/acs.est.0c00695>, 2020.

1020 Rocchi, A., Sotomayor-Garcia, A., Cabrera-Brufau, M., Berdalet, E., Dall'Osto, M., and Vaqué,
 1021 D.: Abundance and activity of sympagic viruses near the Western Antarctic Peninsula, *Polar Biol.*,
 1022 45, 1363–1378, <https://doi.org/10.1007/s00300-022-03073-w>, 2022.

1023 Schoffman, H., Lis, H., Shaked, Y., and Keren, N.: Iron-nutrient interactions within
 1024 phytoplankton, *Front. Plant Sci.*, 7, 1223, <https://doi.org/10.3389/fpls.2016.01223>, 2016.

1025 Sieracki, M. E., Johnson, P. W., and Sieburth, J. M.: Detection, enumeration, and sizing of
 1026 planktonic bacteria by image-analyzed epifluorescence microscopy, *Appl. Environ. Microbiol.*,
 1027 49, 799–810, <https://doi.org/10.1128/aem.49.4.799-810.1985>, 1985.

1028 Spiese, C. E., Kieber, D. J., Nomura, C. T., and Kiene, R. P.: Reduction of dimethylsulfoxide to
 1029 dimethylsulfide by marine phytoplankton, *Limnol. Oceanogr.*, 54, 560–570,
 1030 <https://doi.org/10.4319/lo.2009.54.2.0560>, 2009.

1031 Stefels, J.: Physiological aspects of the production and conversion of DMSP in marine algae and
 1032 higher plants, *J. Sea Res.*, 43, 183–197, [https://doi.org/10.1016/s1385-1101\(00\)00030-7](https://doi.org/10.1016/s1385-1101(00)00030-7), 2000.

1033 Stefels, J., Steinke, M., Turner, S., Malin, G., and Belviso, S.: Environmental constraints on the
 1034 production and removal of the climatically active gas dimethylsulphide (DMS) and implications
 1035 for ecosystem modelling, *Biogeochemistry*, 83, 245–275, <https://doi.org/10.1007/s10533-007-9091-5>, 2007.

1037 Stein, L. Y.: Methylamine: a vital nitrogen (and carbon) source for marine microbes, *Environ.*
 1038 *Microbiol.*, 19, 2117–2118, <https://doi.org/10.1111/1462-2920.13716>, 2017.

1039 Suleiman, M., Zecher, K., Yücel, O., Jagmann, N., and Philipp, B.: Interkingdom cross-feeding of

1040 ammonium from marine methylamine-degrading bacteria to the diatom *Phaeodactylum*
1041 *tricornutum*, *Appl. Environ. Microbiol.*, 82, 7113–7122, <https://doi.org/10.1128/aem.01642-16>,
1042 2016.

1043 Sun, J., Mausz, M. A., Chen, Y., and Giovannoni, S. J.: Microbial trimethylamine metabolism in
1044 marine environments, *Environ. Microbiol.*, 21, 513–520, [https://doi.org/10.1111/1462-](https://doi.org/10.1111/1462-2920.14461)
1045 2920.14461, 2019.

1046 Suttle, C. A.: Viruses in the sea, *Nature*, 437, 356–361, <https://doi.org/10.1038/nature04160>, 2005.

1047 Taubert, M., Grob, C., Howat, A. M., Burns, O. J., Pratscher, J., Jehmlich, N., von Bergen, M.,
1048 Richnow, H. H., Chen, Y., and Murrell, J. C.: Methylamine as a nitrogen source for
1049 microorganisms from a coastal marine environment, *Environ. Microbiol.*, 19, 2246–2257,
1050 <https://doi.org/10.1111/1462-2920.13709>, 2017.

1051 Vaqué, D., Agustí, S., and Duarte, C. M.: Response of bacterial grazing rates to experimental
1052 manipulation of an Antarctic coastal nanoflagellate community, *Aquat. Microb. Ecol.*, 36, 41–52,
1053 <https://doi.org/10.3354/ame036041>, 2004.

1054 Vaultot, D., Courties, C., and Partensky, F.: A simple method to preserve oceanic phytoplankton
1055 for flow cytometric analyses, *Cytometry*, 10, 629–635, <https://doi.org/10.1002/cyto.990100519>,
1056 1989.

1057 Ward, B. B. and Bronk, D. A.: Net nitrogen uptake and DON release in surface waters: importance
1058 of trophic interactions implied from size fractionation experiments, *Mar. Ecol. Prog. Ser.*, 219, 11–
1059 24, <https://doi.org/10.3354/meps219011>, 2001.

1060 Wheeler, P. A. and Hellebust, J. A.: Uptake and concentration of alkylamines by a marine diatom:
1061 effects of H⁺ and K⁺ and implications for the transport and accumulation of weak bases, *Plant*
1062 *physiology*, 67, 367–372, 1981.

1063 Wheeler, P. A. and Kirchman, D. L.: Utilization of inorganic and organic nitrogen by bacteria in
1064 marine systems 1, *Limnology and Oceanography*, 31, 998–1009, 1986.

1065 Wheeler, P. A., North, B. B., and Stephens, G. C.: Amino acid uptake by marine phytoplankters
1066 1, 2, *Limnology and Oceanography*, 19, 249–259, 1974.

1067 Wickham, H.: *ggplot2: Create Elegant Data Visualisations Using Grammar of Graphics*,
1068 Comprehensive R Archive Network (CRAN), 2023.

1069 Wohl, C., Capelle, D., Jones, A., Sturges, W. T., Nightingale, P. D., Else, B. G. T., and Yang, M.:
1070 Segmented flow coil equilibrators coupled to a proton-transfer-reaction mass spectrometer for
1071 measurements of a broad range of volatile organic compounds in seawater, *Ocean Sci.*, 15, 925–
1072 940, <https://doi.org/10.5194/os-15-925-2019>, 2019.

1073 Wohl, C., Villamayor, J., Galí, M., Mahajan, A. S., Fernández, R. P., Cuevas, C. A., Bossolasco,
1074 A., Li, Q., Kettle, A. J., Williams, T., Sarda-Estève, R., Gros, V., Simó, R., and Saiz-Lopez, A.:
1075 Marine emissions of methanethiol increase aerosol cooling in the Southern Ocean, *Sci. Adv.*, 10,

1076 eadq2465, <https://doi.org/10.1126/sciadv.adq2465>, 2024.

1077 Wu, M., McCain, J. S. P., Rowland, E., Middag, R., Sandgren, M., Allen, A. E., and Bertrand, E.
 1078 M.: Manganese and iron deficiency in Southern Ocean *Phaeocystis antarctica* populations revealed
 1079 through taxon-specific protein indicators, *Nat. Commun.*, 10, 3582,
 1080 <https://doi.org/10.1038/s41467-019-11426-z>, 2019.

1081 Yentsch, C. S. and Menzel, D. W.: A method for the determination of phytoplankton chlorophyll
 1082 and phaeophytin by fluorescence, *Deep Sea Res. Oceanogr. Abstr.*, 10, 221–231,
 1083 [https://doi.org/10.1016/0011-7471\(63\)90358-9](https://doi.org/10.1016/0011-7471(63)90358-9), 1963.

1084 Zhang, Q., Jia, S., Chen, W., Mao, J., Yang, L., Krishnan, P., Sarkar, S., Shao, M., and Wang, X.:
 1085 Contribution of marine biological emissions to gaseous methylamines in the atmosphere: An
 1086 emission inventory based on multi-source data sets, *Sci. Total Environ.*, 898, 165285,
 1087 <https://doi.org/10.1016/j.scitotenv.2023.165285>, 2023.

1088 Zu, H., Chu, B., Lu, Y., Liu, L., and Zhang, X.: Rapid iodine oxoacid nucleation enhanced by
 1089 dimethylamine in broad marine regions, *Atmos. Chem. Phys.*, 24, 5823–5835,
 1090 <https://doi.org/10.5194/acp-24-5823-2024>, 2024.